HDL-TR-2010

June 1983

Fluidic Generator to Power a Modular Fuze for a Free-Fall Munition Fuzing System

by Jonathan E. Fine
Carl J. Campagnuolo
CPT Patrick J. Ellis

U.S. Army Electronics Research and Development Command
Harry Diamond Laboratories
Adelphi, MD 20783

The findings in this report are not to be construed as an official Department of the Army position unless so designated by other authorized documents.

Citation of manufacturers' or trade names does not constitute an official indorsement or approval of the use thereof.

Destroy this report when it is no longer needed. Do not return it to the originator.

REPORT DOCUMENTATION PAGE

READ INSTRUCTIONS BEFORE COMPLETING FORM

1. REPORT NUMBER: HDL-TR-2010
2. GOVT ACCESSION NO.:
3. RECIPIENT'S CATALOG NUMBER:

4. TITLE (and Subtitle): Fluidic Generator to Power a Modular Fuze for a Free-Fall Munition Fuzing System
5. TYPE OF REPORT & PERIOD COVERED: Technical Report
6. PERFORMING ORG. REPORT NUMBER:

7. AUTHOR(s): Jonathan E. Fine, Carl J. Campagnuolo, and CPT Patrick J. Ellis (Canadian Air Force Exchange Officer, Eglin AFB, FL 32542)
8. CONTRACT OR GRANT NUMBER(s):

9. PERFORMING ORGANIZATION NAME AND ADDRESS: Harry Diamond Laboratories, 2800 Powder Mill Road, Adelphi, MD 20783
10. PROGRAM ELEMENT, PROJECT, TASK AREA & WORK UNIT NUMBERS: Program Element: 62602F

11. CONTROLLING OFFICE NAME AND ADDRESS: U.S. Air Force, Eglin AFB, FL 32542
12. REPORT DATE: June 1983
13. NUMBER OF PAGES: 44

14. MONITORING AGENCY NAME & ADDRESS (if different from Controlling Office):
15. SECURITY CLASS. (of this report): UNCLASSIFIED
15a. DECLASSIFICATION/DOWNGRADING SCHEDULE:

16. DISTRIBUTION STATEMENT (of this Report): Approved for public release; distribution unlimited.

17. DISTRIBUTION STATEMENT (of the abstract entered in Block 20, if different from Report):

18. SUPPLEMENTARY NOTES: MIPR-FY7621-81-90119; HDL Proj: 489146

19. KEY WORDS (Continue on reverse side if necessary and identify by block number):

Air-driven generator	Battery	Modular fuze	Wind energy for fuze
Fluidic generator	Safing and arming	Bomb fuze	Environmental signature
Power supply	In-line fuze	Wind-driven generator	

20. ABSTRACT (Continue on reverse side if necessary and identify by block number):

A fluidic generator has been developed as a power supply for a modular fuze used in a free-fall munition fuzing system for an Air Force MK-80-series bomb. The fluidic generator was developed in the laboratory to produce 1 W at 1 psi and 2 W at 2 psi within a pop-up housing, so it can be used on high drag bombs. The total operational range of the generator is from 0 to 10 psig.

20. Abstract (cont'd)

A wind tunnel test was conducted to evaluate the fluidic generator's performance when mounted in the MK-84 GBU-10C/B bomb. The test indicated that the fluidic generator can provide electrical energy above the required threshold at the lowest release conditions over the expected range of flight attitudes of the bomb.

The fluidic generator has adequate come-up time to voltage to arm the fuze in the required arming time at the minimum airspeed and lowest release condition.

CONTENTS

FIGURES

FIGURES (Cont'd)

FIGURES (Cont'd)

TABLES

1. INTRODUCTION

A fluidic generator driven by the ram air energy available during flight was developed by Harry Diamond Laboratories (HDL) for a modular bomb fuze. The fuze is being developed for Air Force MK-84 laser-guided bombs (including high drag bombs). The fluidic generator (fig. 1) provides an environmental signature to the fuze.

Safety is achieved in that the generator provides power only after the munition has been intentionally released from the aircraft. This concept ensures that sufficient electrical power is not available until after an intentional release. The fludic generator has no mechanical governing, no moving parts, no bearings, and no lubrication requirements. Hence, it is a reliable power source for the modular fuze system that operates in the environment of a free-fall munition.

The purpose of this report is two-fold:

(1) to describe the development of a fluidic generator to meet the Air Force requirements for the modular bomb fuze, and

(2) to evaluate the results of the fluidic generator performance in a wind tunnel at conditions that correspond to minimum flight release speed.

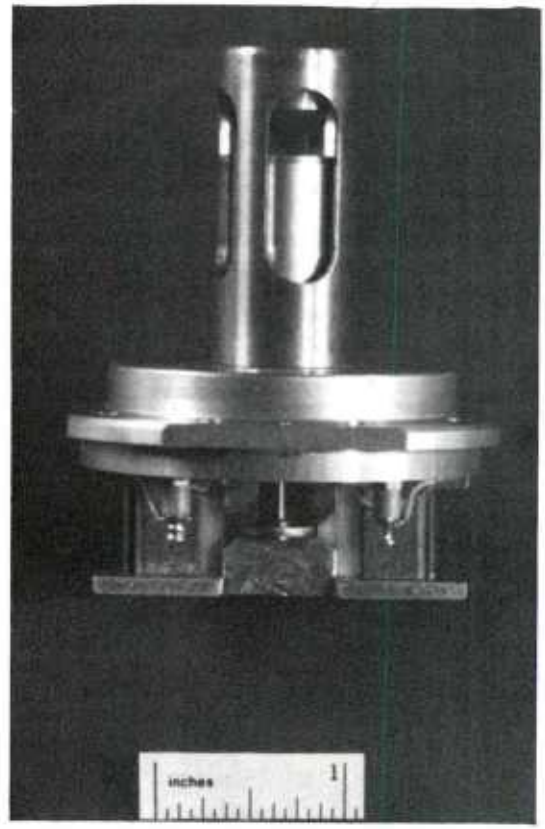

Figure 1. Fluidic generator.

2. REQUIREMENTS

The fluidic generator was developed to meet the power requirements of the fuze for free-fall munitions, including low-speed/low altitude release. The operational envelope for the generator is shown in figure 2, a representative flight envelope for Air Force munitions. Release altitude is plotted versus aircraft Mach number, with the indicated airspeed in knots shown at selected points of the envelope. The airspeed at any two adjacent vertices represents the extreme values for all points between the vertices. The lowest airspeed is 185 knots,* which occurs at Mach 0.65 at 40 kft.† The airspeed remains between 185 and 200 knots for all lower Mach numbers.

---

*knot = 0.51444 m/s

†1 ft = 0.3048 m

The power requirement for the fluidic generator's operation in the low-speed/low altitude regime is the most stringent of the design requirements. The power required of the fluidic generator depends on the time available for charging the system's capacitor during flight, including generator come-up time. At 400 knots (200 m/s) the dynamic pressure is 2 psi.* At this pressure a power of 2.0 W is required from the fluidic generator. At 200 knots (103 m/s--the lowest expected release speed), the dynamic pressure is 1 psi. At this pressure, 1.0 W is required. The effects of decaying airspeed upon activation of the retarding mechanism of high drag weapons must be taken into account when the generator is designed. To meet the requirements over the full profile of figure 2, the generator must operate over a total pressure range from 0 to 10 psig,† and above 2 psig must produce power of no less than 2 W.

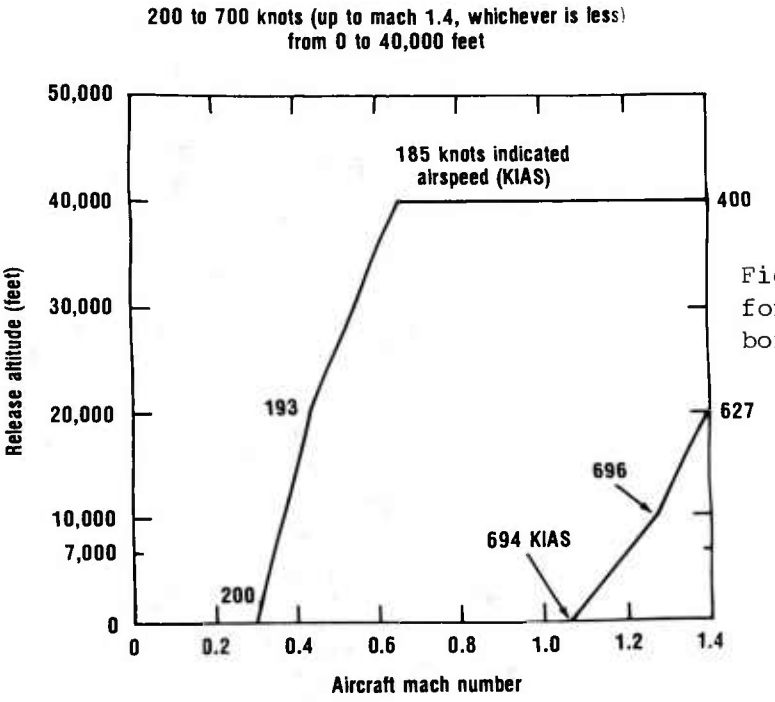

Figure 2. Operational envelope for MK-84 laser-guided high drag bomb.

3. MODULAR FUZE OPERATIONAL CONCEPT

The fluidic generator output is used to drive a transformer with two secondary windings. The lower winding drives a 15-V circuit that charges a 300-μF capacitor, which in turn powers the fuze logic. The upper winding drives a higher-voltage, 50-V circuit which powers the circuitry that provides the electrical arming and detonation functions. The load on each circuit is capacitive while the respective capacitors are being charged, and then becomes resistive. After the bomb is released, the logic circuit begins charging at

1 psi = 6.8947572 × 10^3 Pa

†*psig--differential pressure above ambient atmospheric pressure of 14.7 psi*

the lower voltage. The arming time starts after completion of the internal power-on reset of a microprocessor within the logic circuit, which occurs when 10 to 12 V appears on the capacitor. The fuze come-up time is the time from bomb release that is required for this reset to take place and provides an additional delay to the adjustable arming time.

The arming times are adjustable. The minimum value is 4 s and corresponds to the lowest airspeed release conditions.

4. FLUIDIC GENERATOR DESIGN CONCEPT

The generator design is an offshoot of the fluidic generator used in the M445 time fuze for the Multiple Launch Rocket System (MLRS).[1] This generator is highly reliable since it survives pressures up to 150 psi and stagnation temperatures up to 1000 F* (at rocket burnout), yet provides continuous electrical power throughout a 1 to 2 min flight where altitudes as high as 69,000 ft may be reached. It was felt that the MLRS generator could be made more efficient in terms of power expenditure for the low velocity release conditions while retaining its inherent high reliability.

The fluidic generator converts pneumatic energy (ram air), available along the flight trajectory, into electrical energy. The transformation in energy takes place in three distinct steps:[2] pneumatic to acoustical, acoustical to mechanical, and mechanical to electrical. A schematic of the device is shown in figure 3. As can be seen, ram air passes through an annular nozzle into a conical cavity whose opening is concentric with the annular orifice. The annular jet stream issuing from the orifice impinges on the leading edge of the cavity, creating an acoustic perturbation which triggers air inside the cavity into resonant oscillation. The pulsation of the air within the cavity in turn drives a metal diaphragm (which is clamped about its perimeter at the end of the cavity) into vibration. The vibratory motion of the diaphragm is transmitted to a reed through a connecting rod. The reed is in the air gap between the poles of a magnetic circuit consisting of a pair of permanent magnets between a pair of magnetic keepers (fig. 1). The reed, made of magnetic material, oscillates in the air gap at the system mechanical resonant frequency so that the magnetic flux passing through the reed alternates in direction as the reed approaches and recedes from the opposite poles in the air gap. The resulting alternating flux induces an electromotive force in a conducting coil around the reed. The power generated is mainly a function of the rate of change of the magnetic flux density and the amplitude of the reed excursion in the air gap.

---

[1] *Richard L. Goodyear and Henry Lee, Performance of the Fluidic Power Supply for the XM445 Fuze in Supersonic Wind Tunnels, Harry Diamond Laboratories, HDL-TM-81-4 (February 1981).*

[2] *Carl J. Campagnuolo and Henry C. Lee, Development of a High-Power Fluidic Generator for Hard-Structure Munition (HSM) Bomb, Harry Diamond Laboratories, HDL-TR-1988 (May 1982).*

**°K = (°F + 459.67)/1.8*

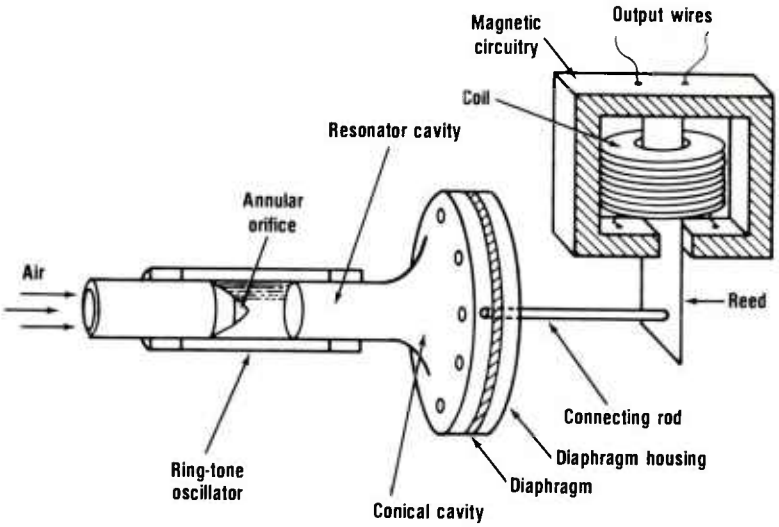

Figure 3. Schematic diagram of fluidic power supply.

5. LABORATORY DEVELOPMENT SUMMARY

5.1 Test Method and Procedures

The generator for the modular bomb fuze is mounted (fig. 4) in a pop-up housing in the rear of the bomb between the fins. The housing is deployed by the removal of a lanyard as the bomb falls away from the aircraft, permitting the inlet duct to "pop up" into the airstream and provide air energy to the generator.

To evaluate the generator's performance in the laboratory, a special adapter was made (fig. 5) that connected the inlet port to an adjustable air supply. The air supply was set to provide a pressure difference across the fluidic generator equal to whatever value was expected in flight. The actual relationship between flight conditions and air energy provided to the generator had to be established through wind tunnel tests.

The development of the fluidic generator was begun while the bomb-well housing was being prepared by the Air Force. Hence, the first generator was evaluated by using the MLRS ogive shown in figure 6. In the MLRS application, the ogive is mounted at the front of the projectile and contains an inlet port at the nose and radial exhaust ports. The air flow to and from the generator is symmetric about the ogive's axis.[3] For laboratory testing, the generator and ogive were held in a test rig as shown in figure 7. The inlet pressure was adjusted by the valve to provide pressure settings within the desired range.

---

[3]*Jonathan E. Fine, Performance of Ram Air Driven Power Supply for Proposed High Altitude Rocket in Naval Surface Weapons Center Supersonic Wind Tunnel, Harry Diamond Laboratories, HDL-TM-80-31 (November 1980).*

Figure 4. Fluidic generator mounted in pop-up housing on bomb.

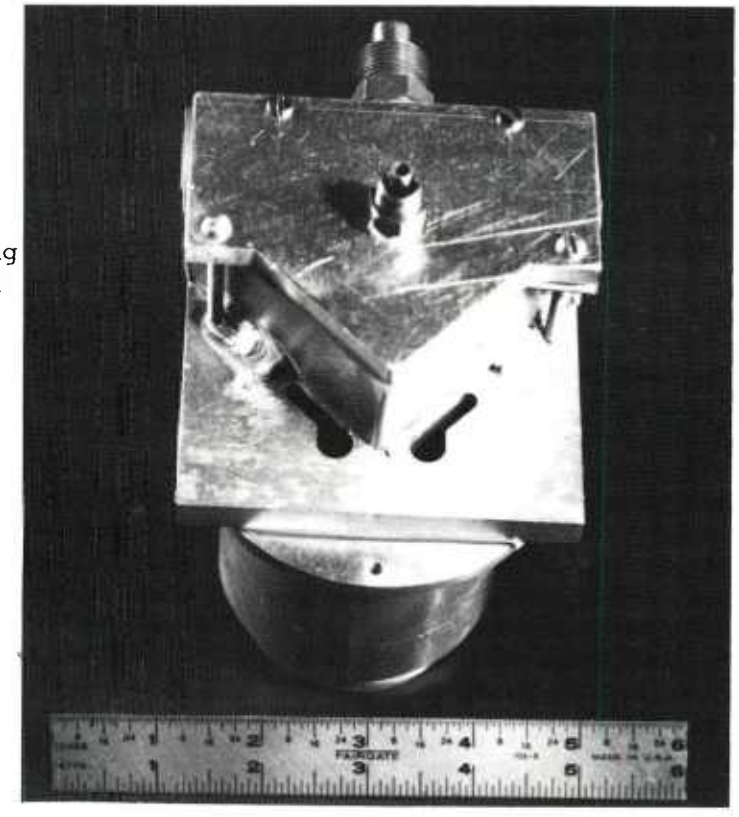

Figure 5. Adapter for evaluating fluidic generator performance in laboratory.

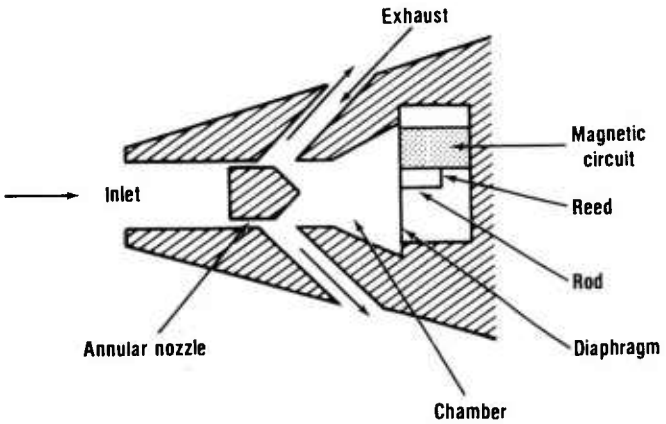

Figure 6. Air passage through ogive containing fluidic generator power supply.

Figure 7. MLRS test rig.

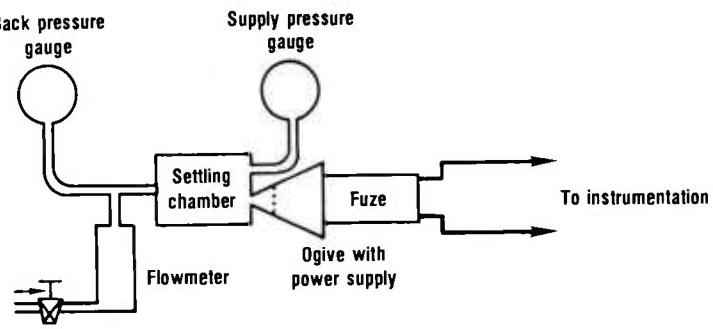

The results of the development effort using the MLRS housing are summarized in figure 8. The output of the initial design was only 0.35 W at 1 psig and 1 W at 2 psig. Development efforts resulted in the improved design that produced 1 W at 1 psig and 2 W at 2 psig. In both cases the electrical load was 2000 ohms. Dimensional differences between the initial and improved designs are also given in figure 8.

The Air Force housing, when completed, was used for subsequent laboratory testing. Figure 9 shows the flow path with the Air Force housing. The airstream is captured in a stagnation chamber and then ducted to the generator and out through exhaust slots. Because of these differences, the flow pattern is no longer symmetrical. As seen from figure 10 (the intermediate design curve), the Air Force housing reduced the output power, compared with the improved design curve in figure 8. Subsequent development efforts which are summarized in the body of the report, were needed to regain the previous output. The efforts culminated in the final design, with output also shown in figure 10. The final design was tested in a laboratory test housing (fig. 11) that closely simulated the pressure and flow characteristics of the Air Force bomb housing.

5.2 Variation of Generator Parameters

A schematic of the experimental arrangement used to test the fluidic generator in the laboratory is shown in figure 12, where an adapter was used

to conduct the air to the Air Force housing. The electrical load of the fuze was simulated by a 2000-ohm resistor in series with a 0.02-μF capacitor. For each inlet pressure the generated power to the load was calculated from observed rms values of load voltage. The power supply was tested in the laboratory at pressures up to 10 psig.

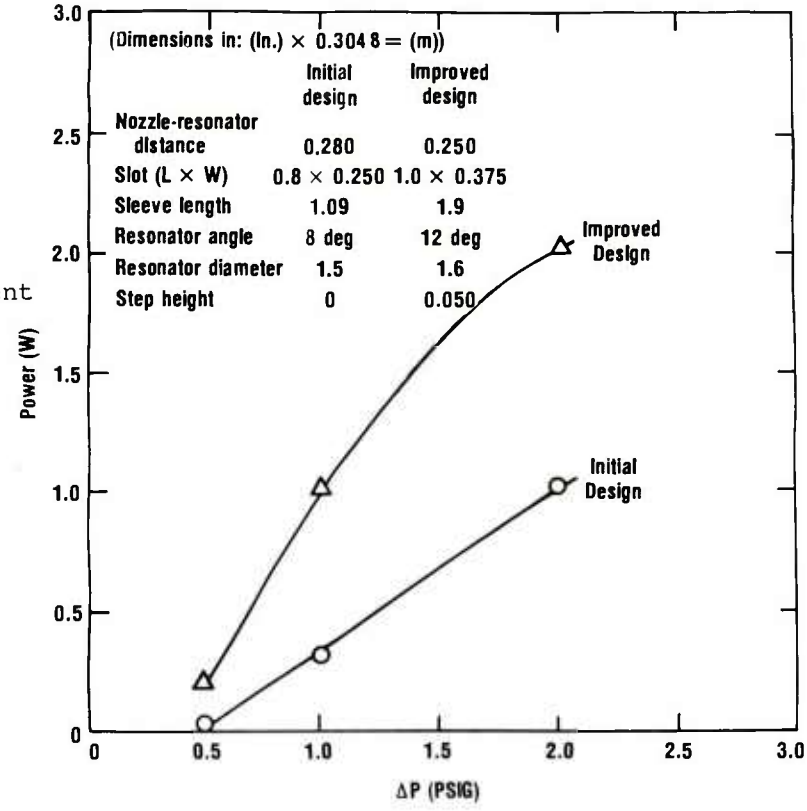

Figure 8. Initial development using MLRS ogive.

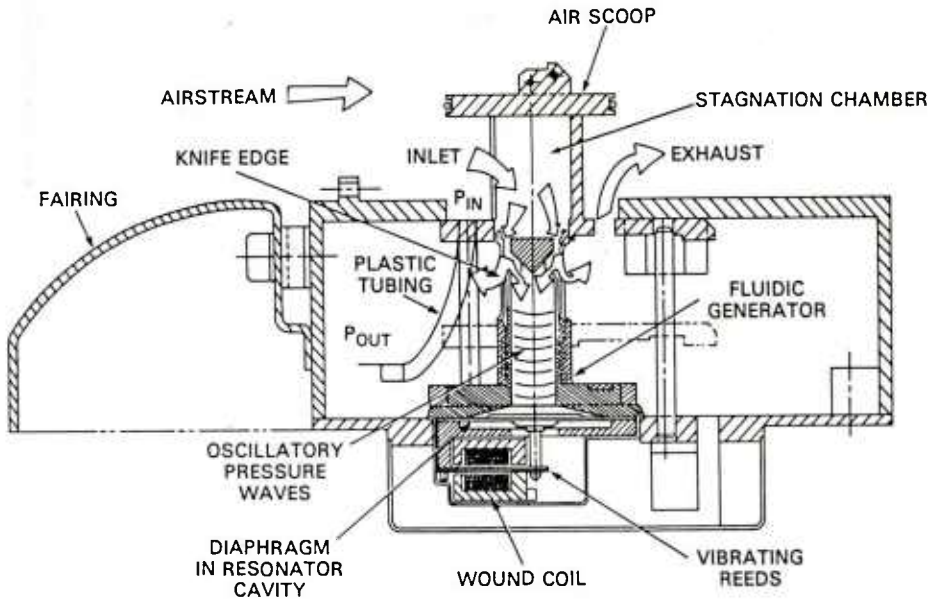

Figure 9. Housing developed by Air Force shown with fluidic generator developed by HDL.

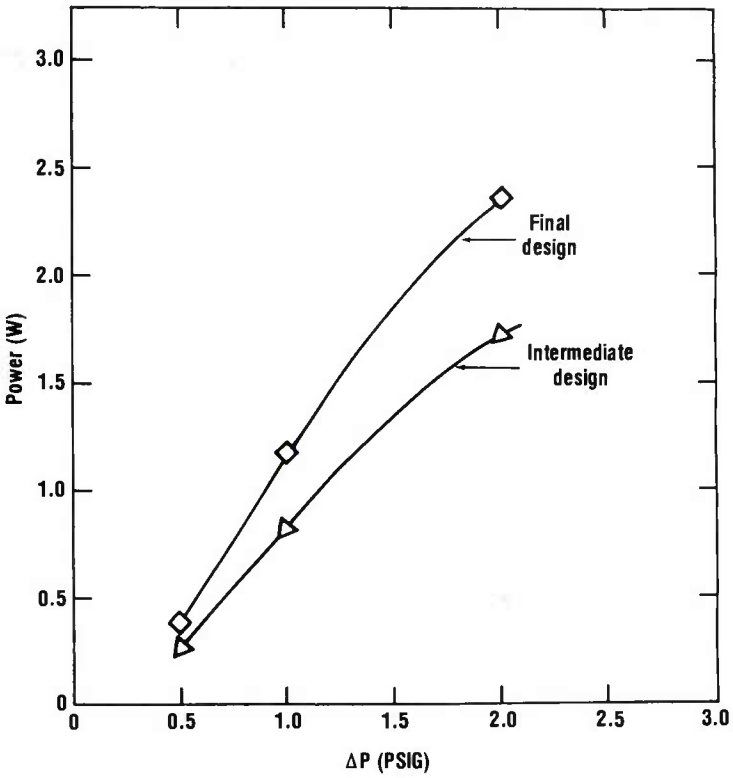

	Dimensions (in.)	
	Intermediate design	Final design
Nozzle-resonator distance	0.250	0.240
Slot (L × W)	1 × 0.375	1 × 0.375
Sleeve length	1.69	1.66
Resonator angle	8 deg	8 deg
Resonator diameter	1.5	1.5
Step height	0	0

Figure 10. Further development results with Air Force test housings.

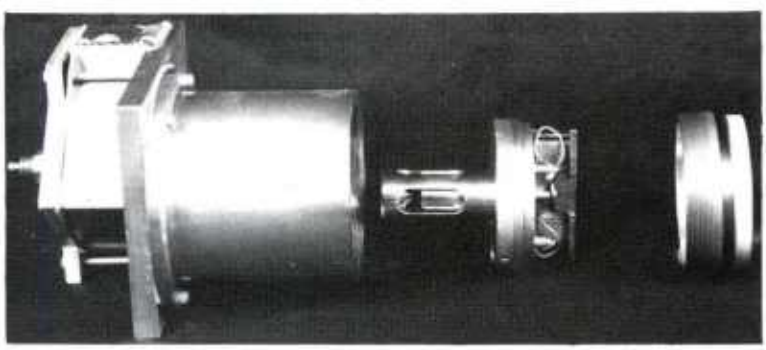

Figure 11. Fluidic generator and laboratory test housing.

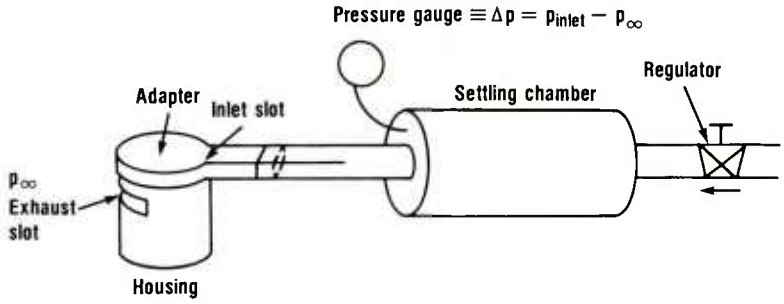

Figure 12. Arrangement for testing Air Force housing in laboratory.

Generator Exhaust Slots.--The fluidic generator parameters that were investigated are shown in figure 13.

The effect of varying the slot width is presented in table 1. The powers for Δp of 0.5 psig, 1.0 psig, and 2.0 psig are tabulated for three slot widths. The slot of 0.375 in. width was optimum. The table shows that further increases in slot width to 0.5 in. reduced the output. Hence, a slot 1 in. long and 0.375 in. wide was retained as being optimum.

Generator Nozzle-Resonator Distance.--The effect of varying the nozzle resonator distance is shown in figure 14, where power output is plotted as a function of pressure up to 2 psig. The power increased noticeably as the nozzle resonator distance was reduced from 0.260 to 0.240 in. Further reduction caused unstable operation (spurious oscillations) at pressures above 2 psig. Hence, 0.240 in. was selected as the minimum value that yields stable operation in the pressure range from 0 to 10 psig.

Resonator Diameter.--The 1.5-in. resonator diameter was far superior to a 1.6-in. resonator diameter, as seen from figure 15, in which electrical power is plotted versus inlet pressure. A reduction of 6.25 percent in diameter caused a 60-percent increase in power at 1 psig and a 44-percent increase at 2 psig. This figure suggests that reducing the diameter further should improve the output even more. This was not done, because it would have required the making of new diaphragms, a much more costly change that would require long lead times.

Resonator Step.--Previous designs employed a resonator with no step. The results of investigating the effect of increasing the step height are presented in figure 16, in which power is plotted versus pressure. As the step was increased from 0 to 0.025 in., the power at 1 psig increased from 0.88 W to 1.3 W; and the power at 2 psig, from 1.90 W to 2.65 W. A further increase in step height, from 0.025 in. to 0.050 in., produced a slight increase in power from 1 to 2 psig, but a larger increase at the lower pressure--0.5 psig. Hence, the 0.050-in. step appeared most promising.

Resonator Angle.--The effect of resonator angle on the power output was evaluated by increasing the angle from 8 to 10 deg. This was done by machining material from the inside of the resonator. The results are shown in figure 17. A drop in power occurred as the angle was increased to 10 deg. Hence, 8 deg was taken as the preferred value. A lesser angle interferes with the diaphragm motion.

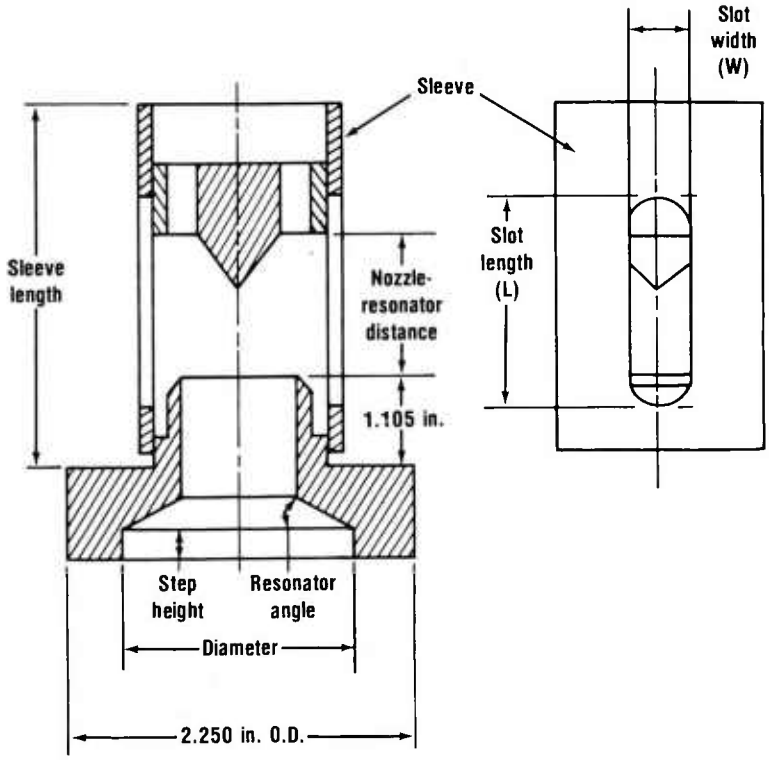

Figure 13. Nozzle-resonator subassembly of fluidic generator showing parameters investigated.

TABLE 1. EFFECT OF SLOT WIDTH ON POWER FROM FLUIDIC GENERATOR TESTED IN AIR FORCE HOUSING

	Inches*
Nozzle-resonator distance	0.240
Sleeve length	1.69
Resonator diameter	1.5
Step height	0
Slot length	1
Resonator angle	8 deg

Electrical Power for Indicated Values of ΔP

Slot width (in.)	ΔP		
	0.5 PSIG (W)	1.0 PSIG (W)	2.0 PSIG (W)
0.375	0.302	0.890	1.90
0.437	0.300	0.865	1.81
0.500	0.288	0.852	1.80

1 in. = 25.4 mm

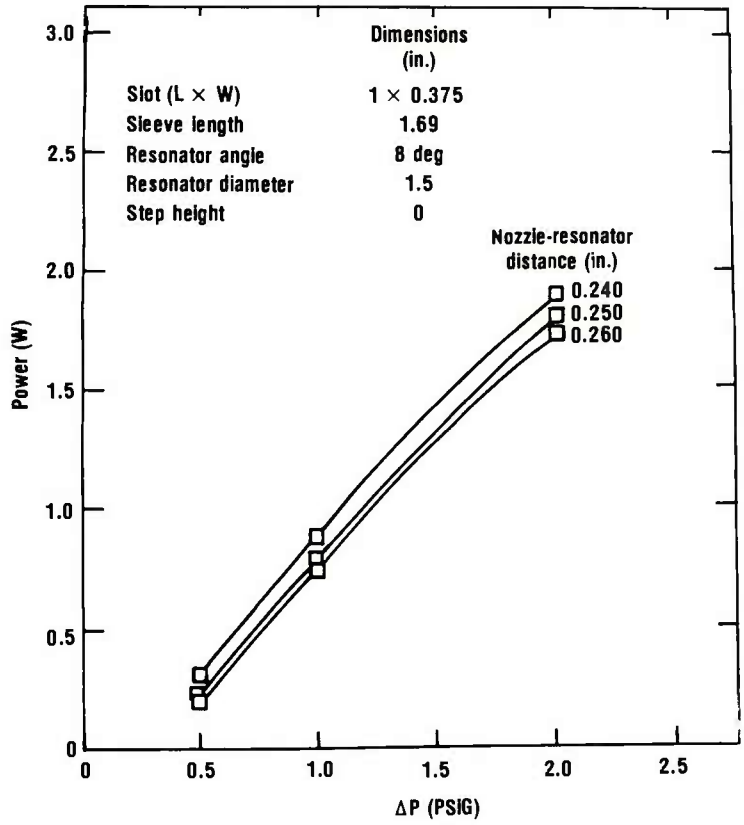

Figure 14. Effect of nozzle-resonator distance on power output of fluidic generators in Air Force housing.

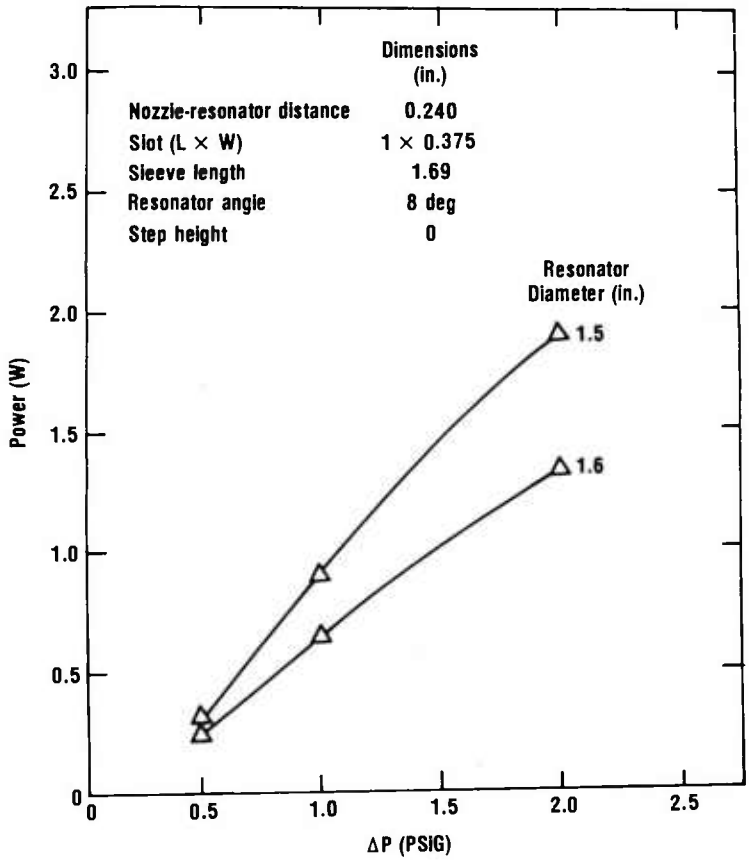

Figure 15. Effect of resonator diameter on power output of fluidic generator in Air Force housing.

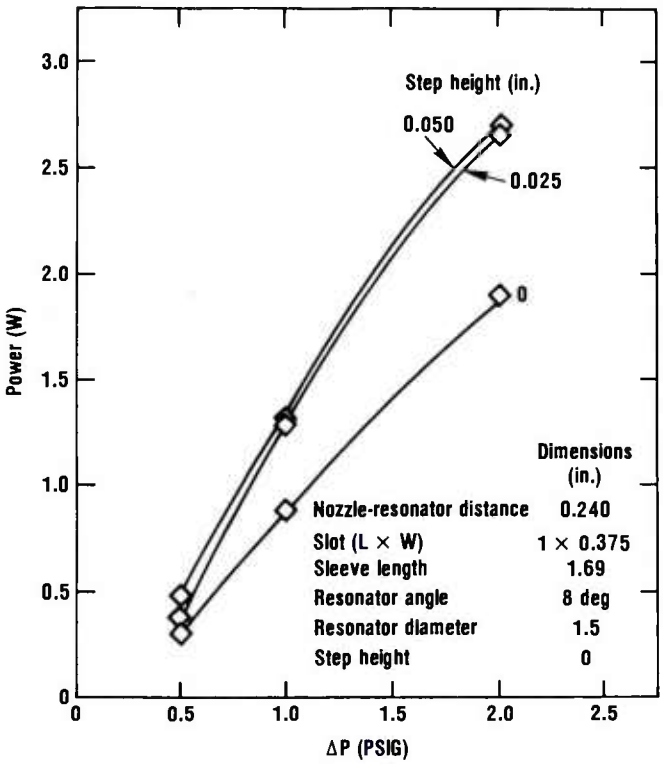

Figure 16. Effect of step height on power produced by fluidic generator in Air Force housing.

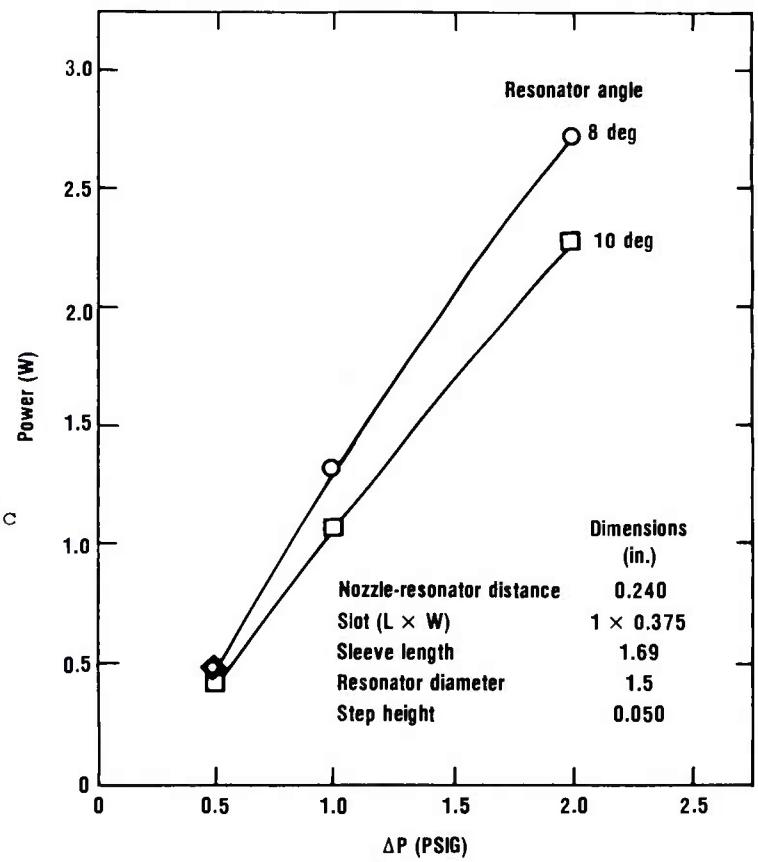

Figure 17. Effect of resonator angle on power output of fluidic generator in Air Force housing.

Final Design in HDL Test Housing.--The above efforts resulted in a design (dimensions shown in fig. 10) that satisfied the power requirements at 1 psig. Twenty-eight generators were tested in a test housing at HDL that closely simulated the pressures and flows in the Air Force housing. The results are shown in figures 18 and 19, in which average power for all 28 generators is plotted versus pressure difference. Minimum and maximum values are also shown.

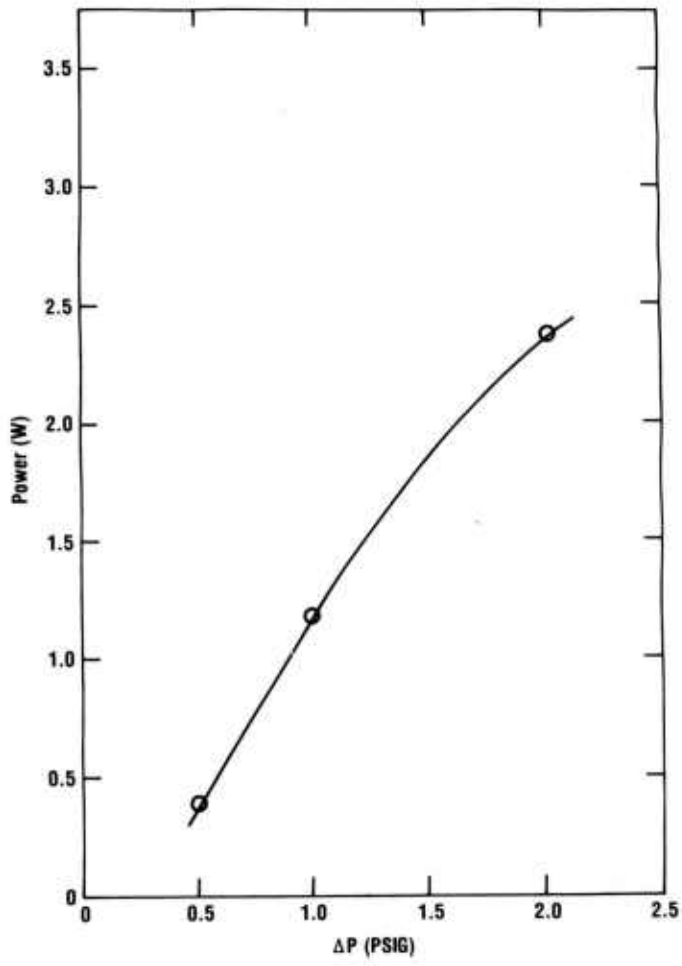

Figure 18. Average values of electrical power for 28 generators of present design tested in HDL test housing.

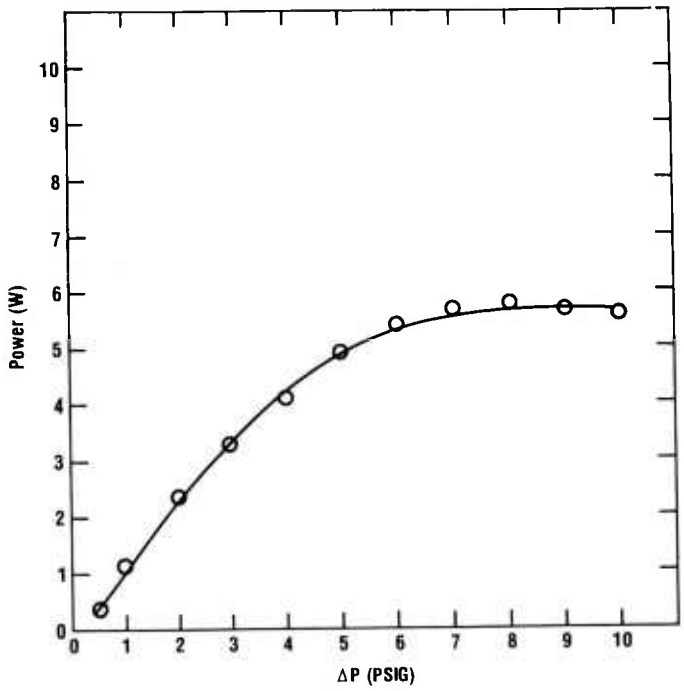

Figure 19. Average values of electrical power for 28 fluidic generators of present design in HDL test housing over working pressure range.

Figure 19 covers the pressure range up to 2 psig. Figure 18 shows that the power supply not only produces the required power at 1 and 2 psig, but also that it operates up to a pressure of 10 psig.

6. WIND TUNNEL TEST

6.1 Objectives

A wind tunnel test was conducted at Arnold Engineering Development Center (AEDC), Tennessee, from 23 to 24 February 1982, to evaluate generator performance at subsonic flight conditions.[4] The generator was installed in a pop-up housing mounted on a bomb that consisted of an MK-84 center body and canards and a GBU-10C/B nose and tail assembly (fig. 20).

The primary objective of this test was to obtain the output voltage and frequency characteristics of the fluidic generator at low air speeds (200 knots). Other objectives were to (1) determine the "start-up" time provided by the generator, (2) define any degradation experienced by the generator due

[4] *R. W. Hobbs, Wind Tunnel Tests of a Modular Fuze at Mach Numbers from 0.20 to 0.50, Arnold Engineering Development Center, AEDC-TSR-82-P7 (March 1982).*

to extended usage, and (3) determine the boundary-layer distribution in front of the generator scoop. Data were obtained at Mach numbers from 0.2 to 0.5 and at free-steam total pressures of 8.3 psia and 16.6 psia.* Angle of attack was varied from -4 to 10 deg at zero roll angle, and roll angle was varied from 0 to -90 deg at angles of attack of 4 and 8 deg. The general arrangement and location of the test article is shown in figure 21. Additional information about the tunnel, its capabilities, and operating characteristics can be found elsewhere.[5]

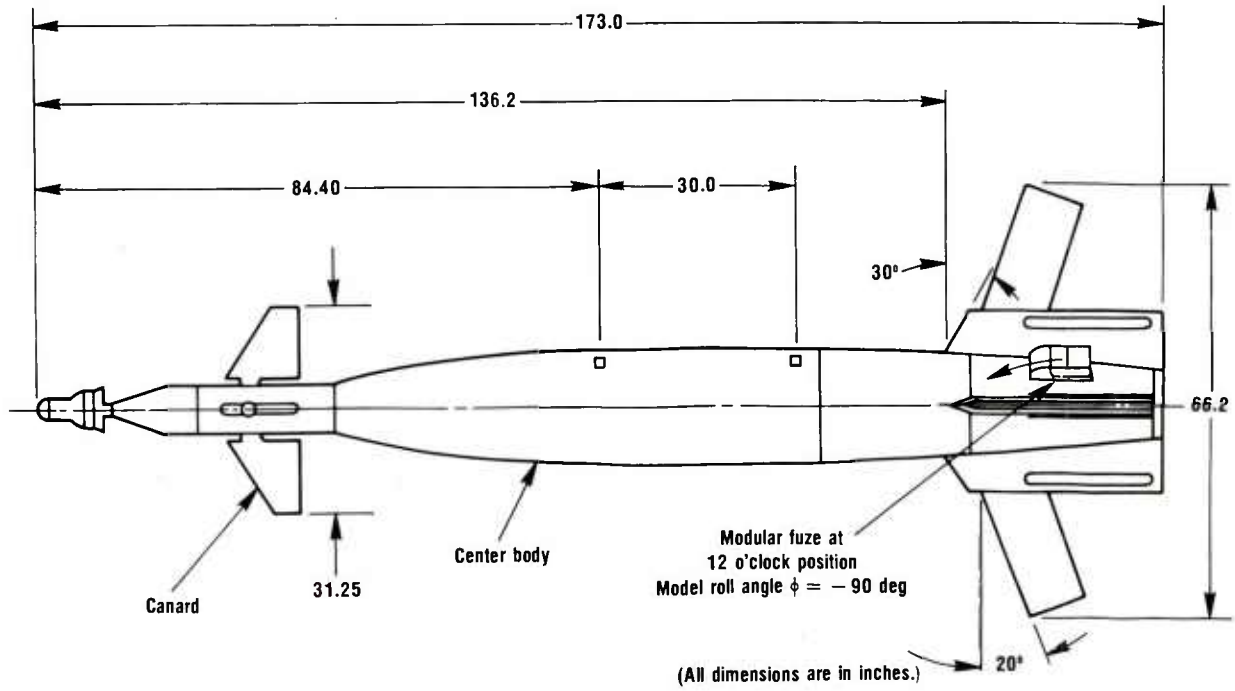

Figure 20. Test article geometry and dimensions.

6.2 Hardware

The test hardware consisted of an MK-84 center body and canards and a GBU-10C/B nose and tail assembly. A modular fuze was mounted between the tail fins with an aerodynamic fairing attached to its front (fig. 22). The test article was mounted on the propulsion wind tunnel (PWT) standard sting support mechanism, as shown in figures 21 and 22. During a special run to measure generator come-up time, a solenoid was used to pull the lanyard that remotely deployed the pop-up housing (fig. 23).

---

[5] *Test Facilities Handbook (Eleventh Edition), Propulsion Wind Tunnel Facility, 4 (April 1981).*

**lb/in.^{2} absolute*

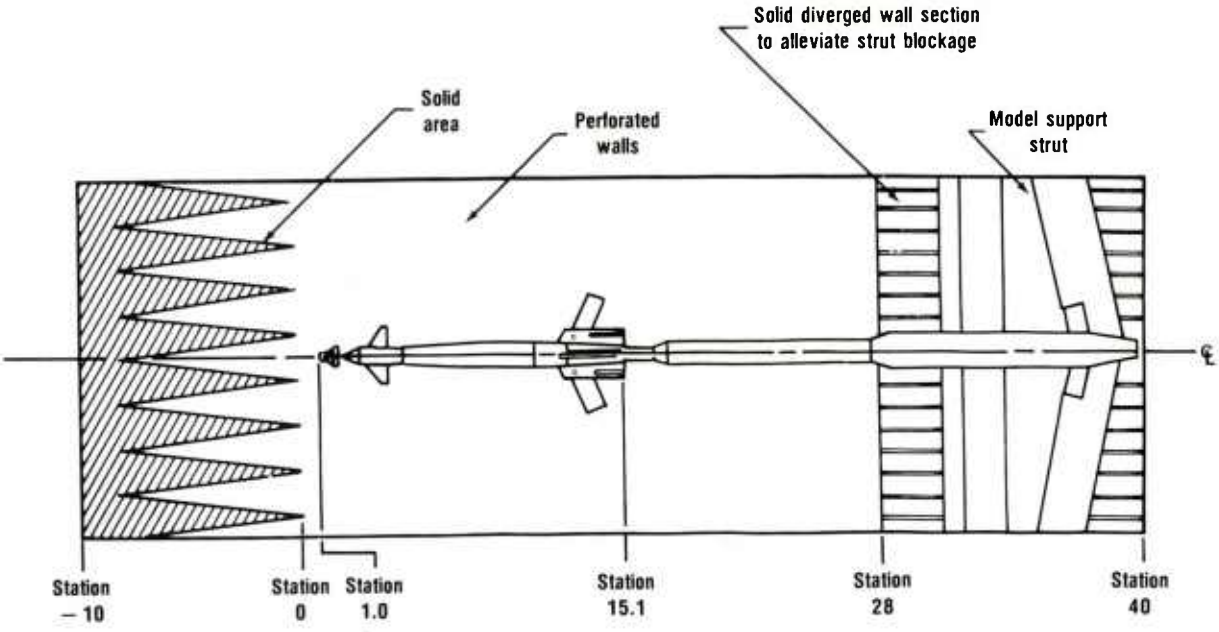

Figure 21. Test article location in tunnel 16T.

Figure 22. Bomb and fuze mounted in wind tunnel.

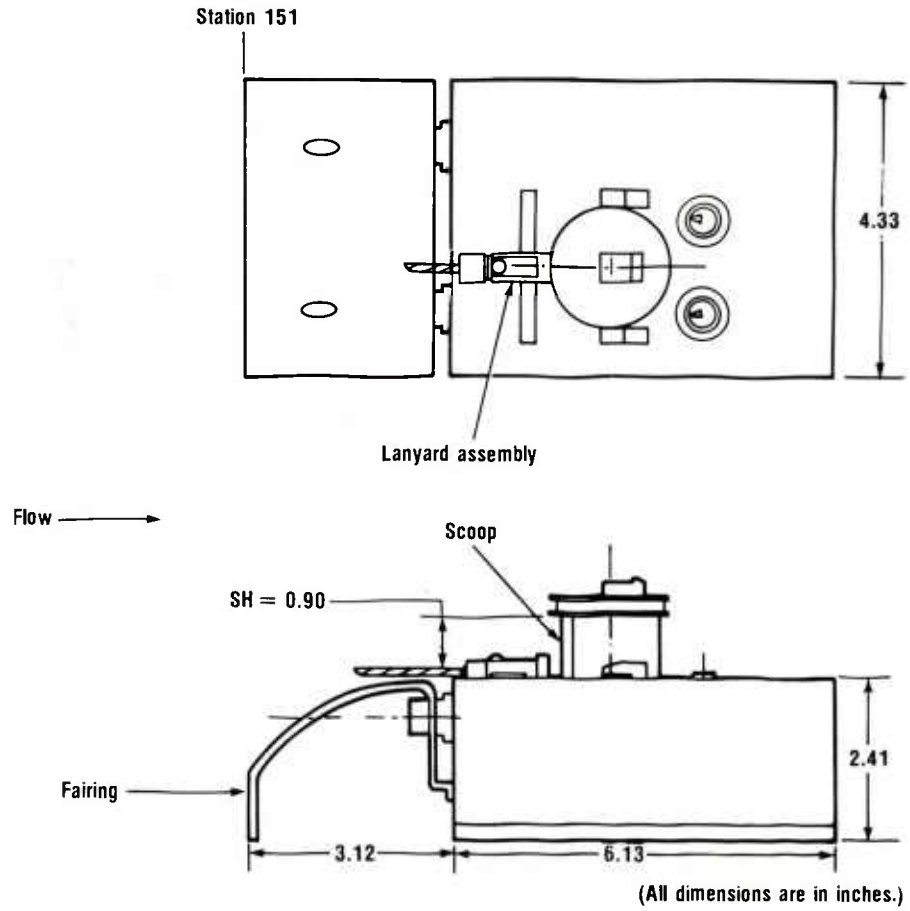

Figure 23. Schematic diagram of pop-up housing showing lanyard assembly.

6.3 Instrumentation

To determine the inlet conditions corresponding to the generator's output, a pressure rake was used to obtain the boundary-layer distribution in front of the generator scoop. The rake contained one static pressure orifice and 13 total pressure probes connected to pressure transducers (fig. 24 and 25). The rake was attached to a simulated fairing and mounted 180 deg away from the modular fuze.

A pressure transducer was mounted inside the fluidic generator to measure the static pressure difference in the generator cavity. The static pressure difference was used to define any generator degradation due to extended usage by a comparison of the output voltage at similar pressure differences. Sting pitch and roll angles were measured by synchrotransmitters. The test article angle of attack and the roll angle were measured by electronic-pendulum angle sensors. The output voltage and frequency, the generator cavity differential static pressure, and the two "event" marks for measuring come-up time were recorded continuously on magnetic tape. Data were transmitted to an IBM-370 computer for on-line data evaluation and comparative analysis using an interactive graphics system.

An AC voltage across a 2000-ohm electrical load was furnished to the instrumentation.

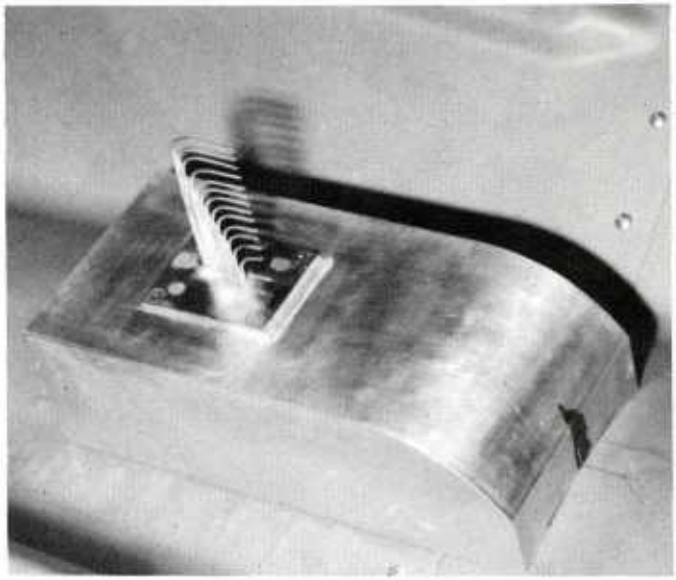

Figure 24. Rake mounted on fairing for boundary layer measurements.

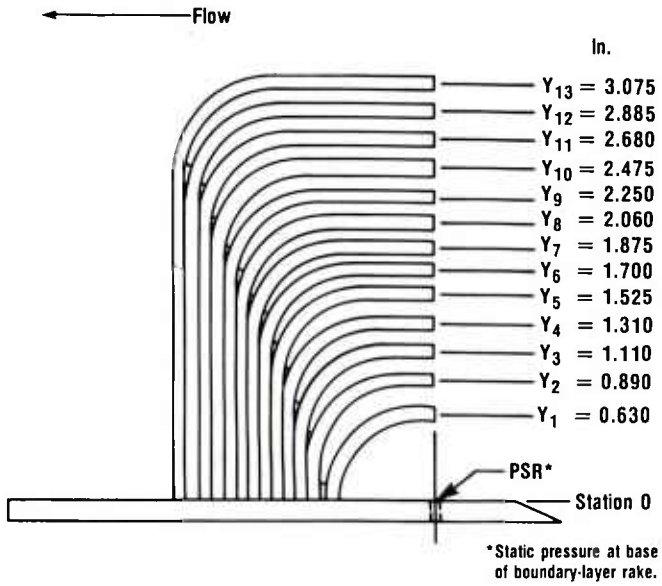

Figure 25. Drawing of rake showing location of pressure probes.

6.4 Analysis of Boundary Layer Rake Data

The boundary layer rake was used to obtain a total pressure profile above the modular fuze housing to insure that the pop-up fluidic generator housing was properly positioned in the air stream and to determine the effect of flight conditions and vehicle attitude on the positioning. To do this, the rake was positioned on a fairing identical in size and contour to the modular fuze housing with the pop-up in the retracted position. A close-up of the

modular fuze with pop-up retracted is shown in figure 26. (The rake is shown in fig. 24.) The rake was 180 deg from the fuze, and had the same orientation relative to the canards. Thus, the flow pattern at the rake corresponded to the flow pattern of the fuze at zero angle of attack. At nonzero angles of attack, the fuze was positioned antisymmetrically to the rake. Therefore, at that angle of attack, the bomb had to be rolled 180 deg to obtain the profile corresponding to the fuze location.

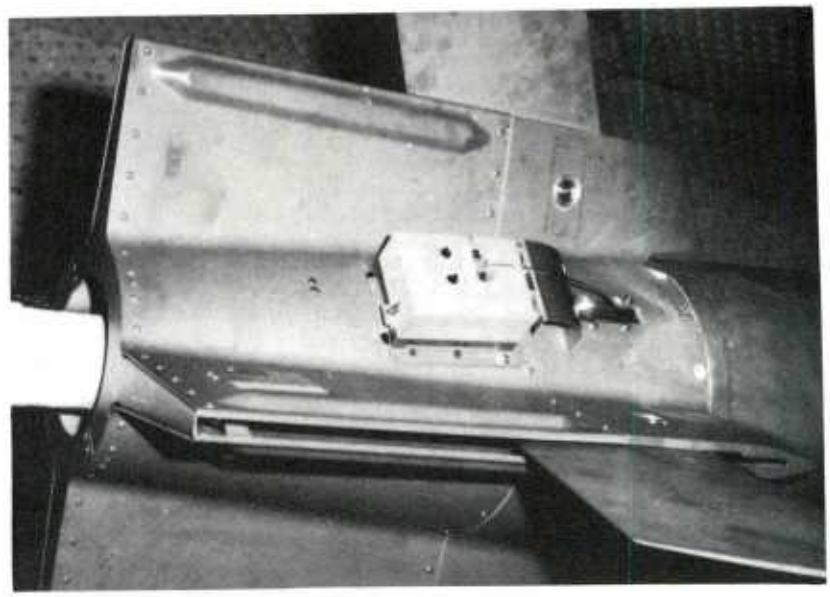

Figure 26. Modular fuze on bomb with pop-up housing retracted.

Figure 27 is a closeup of the modular fuze with the pop-up housing deployed. The scoop inlet that conducts air to the generator is 0.9 in. above the fairing.

As shown in figure 25, the rake consists of 13 total pressure probes located from 0.630 to 3.075 in. above the fairing. A static pressure tap is located at the fairing surface. A typical pressure profile is shown in figure 28, consisting of the total pressure values at each probe for wind tunnel conditions of Mach 0.30, PT = 16.6 psia, 0 deg angle of attack, and -90 deg roll. The probe height above the fairing is the ordinate, and the total pressure at the probe is shown as the abscissa. The pressure increases from 15.5 psia at probe Y1 at 0.69 in. from the surface to 16.66 psia, the free stream value at probe Y5, 1.525 in. from the surface. The pressure remains constant at 16.6 psia for all probes further from the surface. The boundary layer height is the closest point to the surface at which the total pressure is nearly equal to the free stream value, and corresponds to the knee of the curve. The static pressure at the surface, PSR, 15.37 psia, is lower than the free stream static pressure, P, 15.65 psia (fig. 28).

The local Mach number is a function of the total pressure of the probe and the static pressure at the surface, and was calculated from the isentropic formula:

$$M_{Local} = \sqrt{\left(\frac{2}{\gamma - 1}\right)\left[\left(\frac{P_{PSR}}{P_{HBLN}}\right)^{-\left(\frac{\gamma - 1}{\gamma}\right)} - 1\right]} = \sqrt{5\left[\left(\frac{P_{PSR}}{P_{HBLN}}\right)^{-0.28571} - 1\right]} ,$$

where γ = specific heat capacity ratio = 1.4 for air,
P_{PSR} = static pressure at fairing surface (fig. 28), and
P_{HBLN} = total pressure at the probe (fig. 28).

Local Mach number rather than total pressure profiles is used to determine the boundary layer thickness because the local Mach number is proportional to the air velocity near the bomb.

The local Mach number calculated as a function of probe height from the pressure data of figure 28 is plotted in figure 29. The curve has the same shape as the pressure profile. The Mach number increases with height up to a knee, and remains constant at a maximum Mach number for all greater heights. The maximum local Mach number is slightly higher than the free stream value because of the lower static pressure used in the above calculations. The boundary layer height is defined as the distance above the fairing where the local Mach number is 95 percent of its maximum value. This furnishes the same value (1.1 in.) for the boundary layer thickness as the knee of the pressure profile. These values were calculated for a range of wind tunnel parameters and vehicle angles of attack. The results are summarized in table 2 and are discussed below.

The boundary layer height as a function of flight Mach number for zero angle of attack, -90 deg roll, and 8.33 psia total pressure was obtained from the local Mach profiles, and the results are included in table 2. The

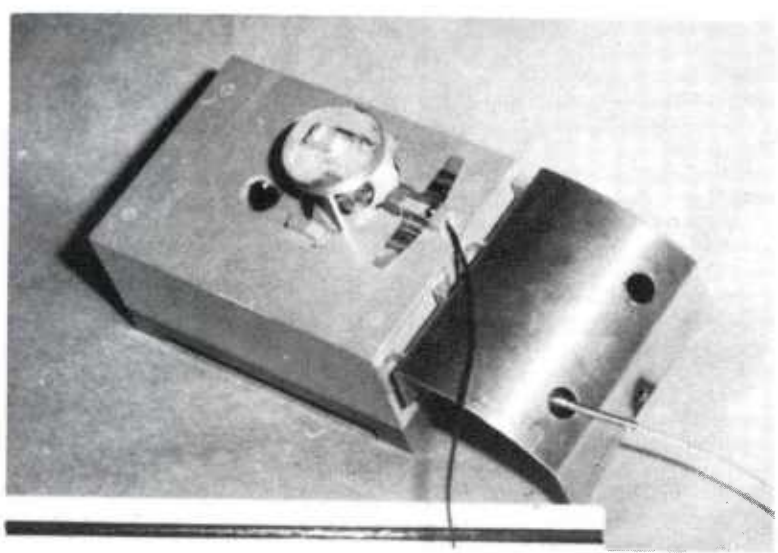

Figure 27. Modular fuze on bomb with pop-up housing deployed.

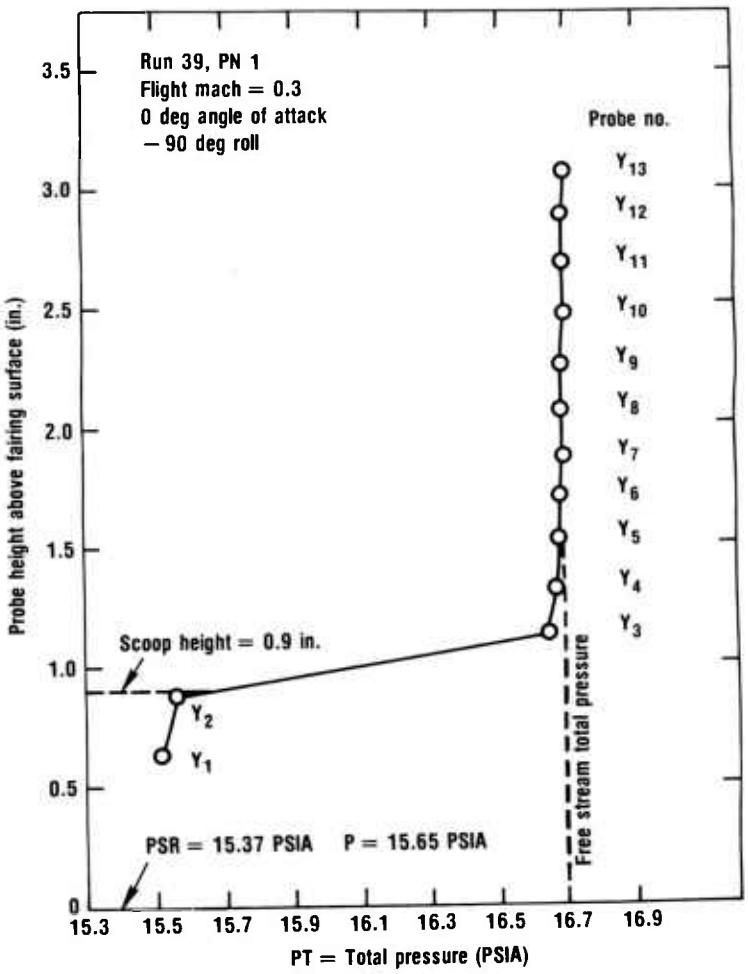

Figure 28. Typical pressure profile.

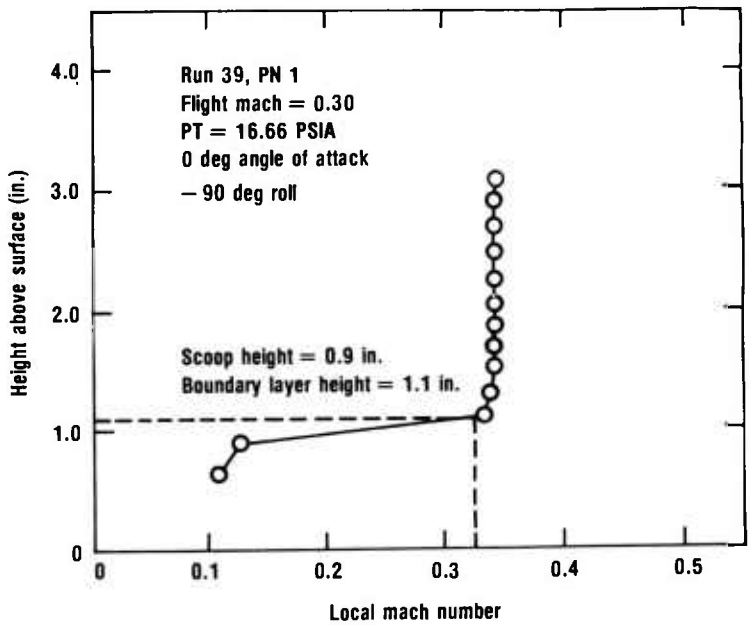

Figure 29. Local Mach number calculated for typical pressure profile as function of probe height.

boundary layer height remains constant with Mach number, at 0.9 in. from Mach 0.2 to Mach 0.5. The scoop entrance is at 0.9 in., which is just at the outer edge of the boundary layer.

TABLE 2. SUMMARY OF EFFECT OF MACH NUMBER, TOTAL PRESSURE, AND ANGLE OF ATTACK ON BOUNDARY LAYER HEIGHT FOR 0 DEG ROLL ANGLE

Run number	Point number	Angle of attack (deg)	Total pressure (PSIA)	Mach number	Boundary layer height (in.)
Effect of Mach number					
17	4	0	8.33	0.2	0.87
16	4	0	8.33	0.3	0.88
15	1	0	8.33	0.4	0.90
14	4	0	8.33	0.5	0.88
Effect of total pressure					
15	1	0	8.33	0.4	0.9
40	3	0	16.66	0.4	1.1
Effect of angle of attack					
40	3	0	16.66	0.4	1.1
40	9	+8	16.66	0.4	1.34
43	6	-8	16.66	0.4	1.08

The effect of increasing the total pressure to 16.66 psia at Mach 0.4 can be seen in table 2. The boundary layer height is again constant with Mach number, but has a higher value of 1.1 in. at 16.66 psia compared with 0.9 in. at 8.33 psia. Thus, the two-fold increase in total pressure has only a slight effect on the boundary layer thickness.

The angle of attack does affect the boundary layer height, as shown in table 2. This angle corresponds to the extreme values of -8, 0, and +8 deg. For -8 and 0 deg the boundary layer height was the same--1.1 in. As the fuze is tilted away from the flow to +8 deg, the boundary layer height increases to 1.34 in. For these cases, the scoop height of 0.9 in. is within the boundary layer. In summary, the raising of the scoop height to 1.4 in. would place the inlet above the boundary layer for all wind tunnel conditions and angles of attack tested.

6.5 Pressure Recovery in Fluidic Generator Housing

A transducer was mounted in the fluidic generator housing to measure the differential pressure (PFG = P_{IN} - P_{OUT}) across the fluidic generator (fig. 9). This pressure should correspond closely to the gauge pressure, Δp, measured in the HDL test housing in the laboratory (fig. 12).

The pressure, Δp, in the wind tunnel housing (PFG) is plotted versus free stream dynamic pressure, q_1, for three angles of attack in figures 30, 31, and 32, for total pressures of 8.33 and 16.66 psia.

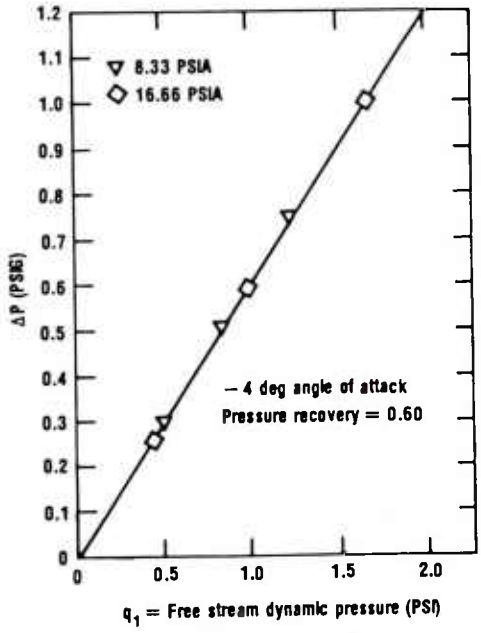

Figure 30. Pressure recovery of pop-up housing at -4 deg angle of attack.

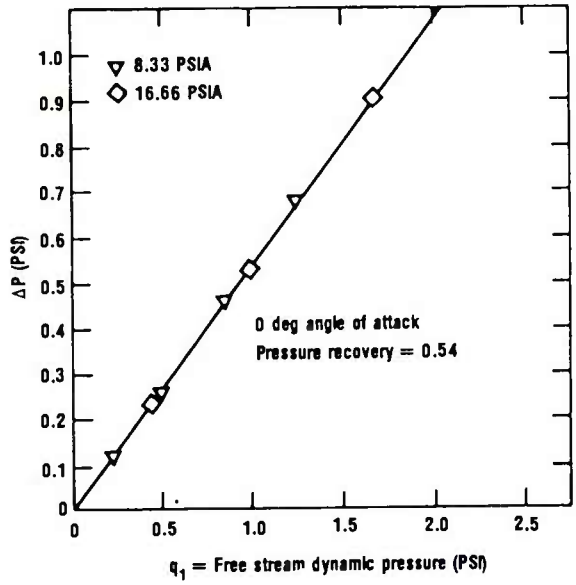

Figure 31. Pressure recovery of pop-up housing at 0 deg angle of attack.

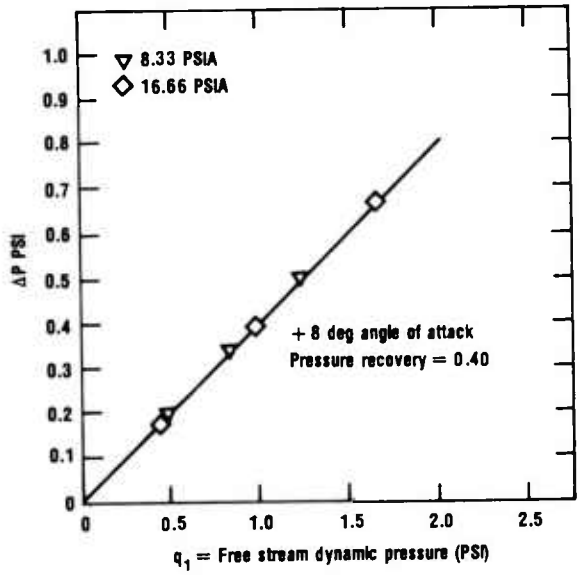

Figure 32. Pressure recovery of pop-up housing at +8 deg angle of attack.

At a -4 deg angle of attack, the data for both values of total pressure fell on the same straight line through the origin, with a slope of 0.60. The slope (pressure recovery) is defined as the fraction of the free stream dynamic pressure that appears across the generator. The pressure recovery was independent of total pressure. The same observation was made for angles of attack of 0 deg and +8 deg, where the pressure recoveries were 0.54 and 0.40, respectively.

In summary, for different angles of attack, the pressure recovery was independent of total pressure and decreased with increasing angle of attack, because the scoop is tilted further from the free stream.

6.6 Come-up Time

The generator come-up time* to 12 Vdc was measured in the wind tunnel at the minimum airspeed release condition. For this test, the simulated fuze circuit (fig. 33) was used. Because at least 12 Vdc are needed to start the timers in the timing circuit, the come-up times with the simulated fuze circuit were measured with a timer having an operational threshold of 12 Vdc. The fluidic generator come-up time was measured for the low airspeed release condition of 200 knots indicated air speed. To simulate this condition, the wind tunnel was set to operate at Mach 0.5 and at total pressure P_t = 8.33 psig. Then the pop-up housing, which had been held in the retracted position, was deployed by use of a remotely controlled lanyard assembly. The time that it took for the scoop to extend was recorded while the voltages on each of the two load circuits (timing circuit and arming circuit) were being measured as a function of time.

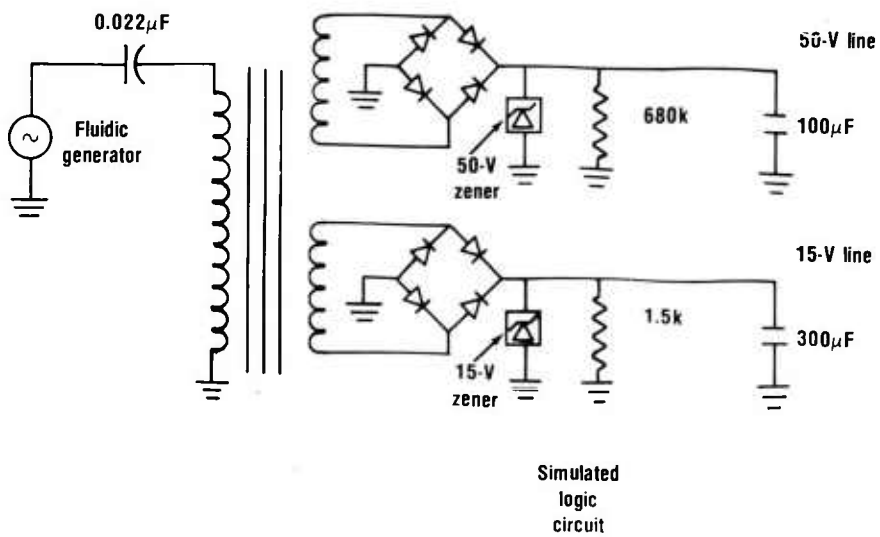

Figure 33. Simulated fuze circuit used on come-up time test.

Come-up time is the time for the logic circuit to activate after the scoop has been deployed. Once the logic circuit has been activated the arming sequence begins. The arming time is the time that starts with logic turn-on and ends when the detonator circuit is enabled. The latter requires about 40 V. The arming time can be changed for each weapon's mission, but is at least the 4 s that is required for the minimum release condition.

The measured come-up time to 12 V was approximately 0.5 s for the low speed drops, and decreased for the higher airspeed release conditions. The measured time for the arming circuit to achieve an operational level of 40 V was approximately 2.15 s, including the 0.5 s come-up time. This gave a margin of 1.85 s for the 4 s arming time.

In summary, the power output from the fluidic generator was sufficient under the minimum air speed release conditions to arm the fuze well in advance of the required arming time of 4 s.

6.7 Fluidic Generator Performance With RC Load at Various Wind Tunnel Conditions and Bomb Attitudes

The fluidic generator output voltage was measured across a 2 kohm resistor connected in series with a 0.02 μF capacitor (fig. 34). This load was also used in laboratory tests at HDL, to permit comparison of laboratory and wind tunnel generator performance. In the wind tunnel, timer turn-on occurred at 15 Vrms. The fluidic generator performance in the wind tunnel is given in figures 35 to 39.

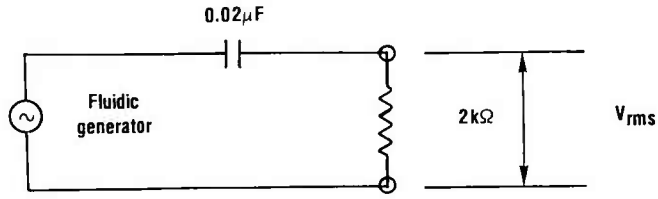

Figure 34. Electrical circuit for measuring fluidic generator output as a function of Mach number and vehicle attitude.

Figure 35. Effect of angle of attack on fluidic generator voltage, PT = 8.33 PSIA.

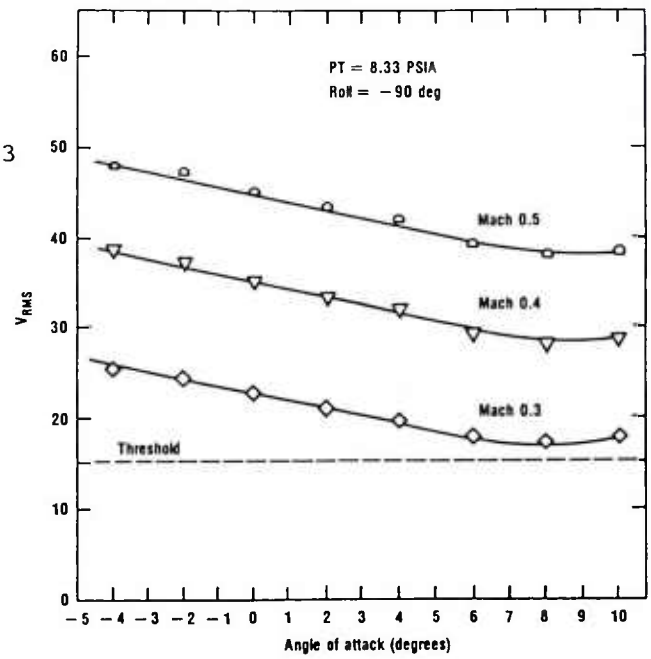

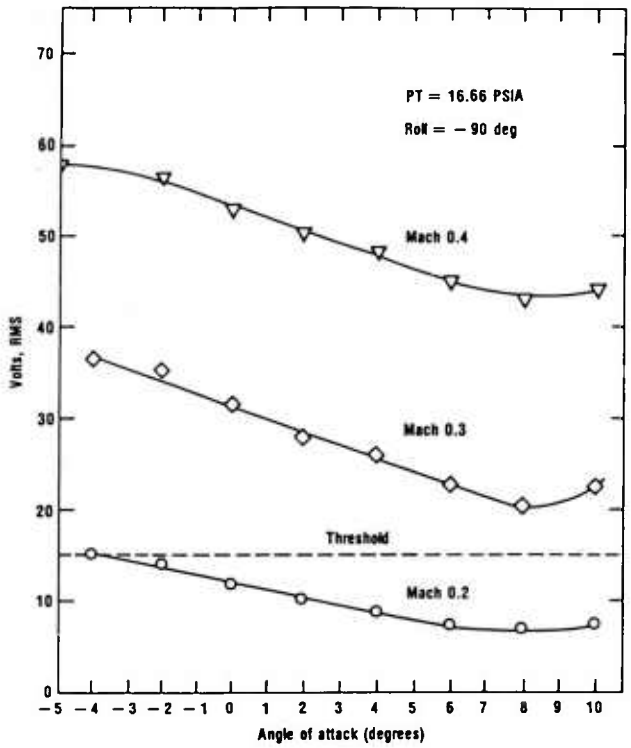

Figure 36. Effect of angle of attack on fluidic generator voltage, PT = 16.66 PSIA.

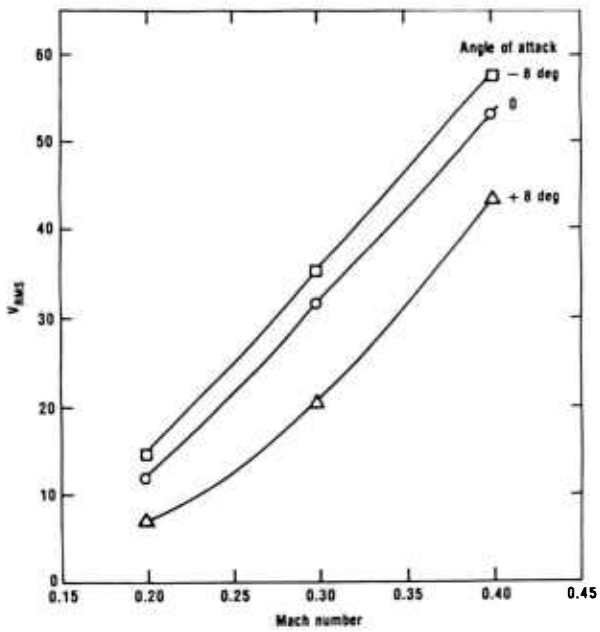

Figure 37. Effect of angle of attack on fluidic generator output, PT = 16.66 PSIA.

Changes of generator voltage at angles of attack from -4 deg to +10 deg at total pressure of 8.33 psia are shown in figure 35. The largest voltage, at a Mach given number, was obtained at the largest negative angles of attack when the scoop was tilted into the flow. The voltage decreased linearly with increasing angle of attack up to +6 deg, and remained at that level up to +10 deg, as the scoop was tilted away from the flow. This corresponds to the increase in boundary layer thickness at the higher angles of attack noted previously. It is seen from the graphs that for any given angle of attack, higher voltage is obtained at higher Mach numbers. Note that for all conditions of Mach number and attitude the required threshold voltage (15 Vrms) was exceeded.

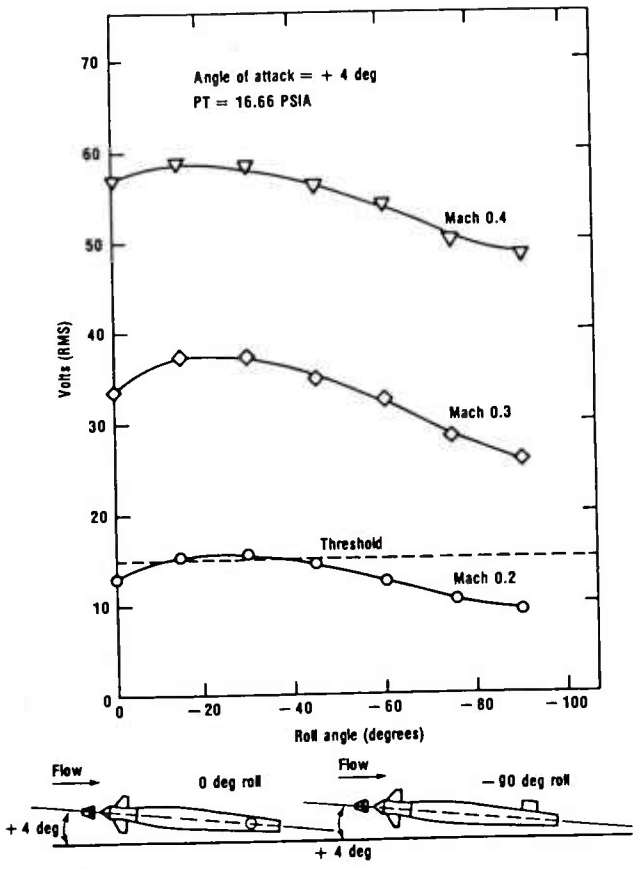

Figure 38. Effect of roll angle on fluidic generator voltage at +4 deg angle of attack.

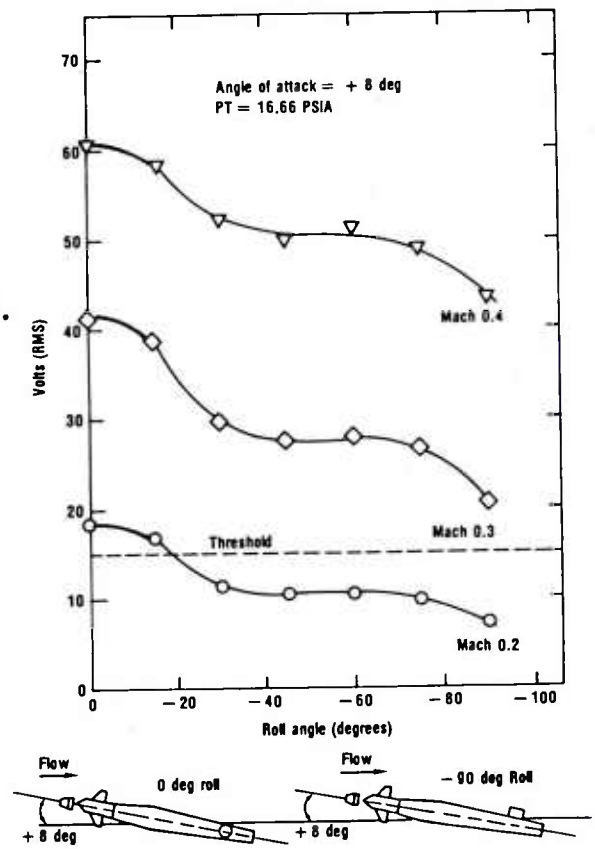

Figure 39. Effect of roll angle on fluidic generator voltage at +8 deg angle of attack.

Figure 36 is the voltage data obtained for total pressure of 16.66 psia. Note that the same trends were observed as with pressures of 8.33 psia; however, the output voltage levels increased proportionally more with Mach number than was the case for 8.33 psia. For example, at 0 deg angle of attack, as the Mach number increased from 0.3 to 0.4, the voltage output increased from 31 to 53 V, an increase of 71 percent. By contrast, from figure 35, at 8.33 psia the voltage increased from 22.7 to 35 V, an increase of only 54 percent, for the same Mach number change.

The effect of angle of attack and Mach number on output voltage is summarized in figure 37. Generator voltage obtained at a total pressure of 16.66 psia is plotted versus Mach number for the extreme values of angle of attack -8 deg, 0 deg, and +8 deg. The figure shows that the percentage reduction in voltage at the extreme angles of attack was greater as the Mach number decreased.

The effect of roll angle is shown in figure 38 for +4 deg angle of attack, and in figure 39 for +8 deg angle of attack. On each figure the orientation of the fuze at the two extreme roll angles of -90 deg and 0 deg is shown. Note that the scoop is mounted vertically at -90 deg roll so that increasing angle of attack in the positive (+) direction tilts the scoop away from the direction of flow.

The threshold voltage of 15 Vrms was achieved for all attitudes above Mach 0.3 and for PT = 16.66 psia. At +4 deg angle of attack (fig. 38) the lowest voltage at any Mach number occurs at -90 deg roll, which corresponds to the maximum shielding of the fuze from the air stream by the bomb. The voltage increased to a maximum as the bomb was rolled counter-clockwise from an angle of -90 deg to -20 deg. The output voltage remained constant for about 15 deg, and decreased as the roll angle dropped to 0 deg. At Mach 0.4, the output voltage increase was from 48 V, at -90 deg, to 59 V, at -20 deg, an increase of 23 percent. At +8 deg angle of attack (fig. 39), the shape of the curve was different due to the greater shielding of the flow by the bomb. The maximum shielding occurs at -90 deg. For Mach = 0.4 the voltage increased from 43.5 -V at -90 deg to 60.5 -V at 0 deg, an increase of 39 percent. From the above, it appears that the effect of roll angle is more pronounced at greater angles of attack.

7. EXPECTED PERFORMANCE OF FLUIDIC GENERATOR IN FLIGHT BASED ON WIND TUNNEL RESULTS

This section shows that the fluidic generator output, as measured in the wind tunnel, is sufficient to power the modular fuze at the low airspeed flight condition, described by the flight envelope of figure 40.

To facilitate comparison of wind tunnel and flight envelope conditions, the free stream total pressure and free stream dynamic pressure, q_1, are also shown at each vertex of the flight envelope. The total pressure varies from 3.6 psia at 40 kft and Mach 0.60, to 15.6 psia at sea level and Mach 0.3. The two values of PT of 8.33 and 16.66 psia were chosen as typical of the range of

release conditions on the portion of the flight envelope corresponding to the minimum indicated airspeed. The values of dynamic pressure (q_1) over this portion of the envelope vary from 0.80 psi to 0.925 psi, and this range is fully covered by the wind tunnel test conditions selected, as shown by table 3. This figure compares the indicated airspeed and dynamic pressure (q_1) for each of the wind tunnel conditions. The wind tunnel conditions were chosen such that values of q1 and indicated airspeed went beyond the values shown on the required envelope. By referring to the curves of generator voltage versus q_1 for 0 deg angle of attack (fig. 41), it is shown that for values of q_1 of 0.8, the minimum value on the flight envelope, voltages above 25 V (rms) are obtained. This is well above the required threshold value of 15 V (rms).

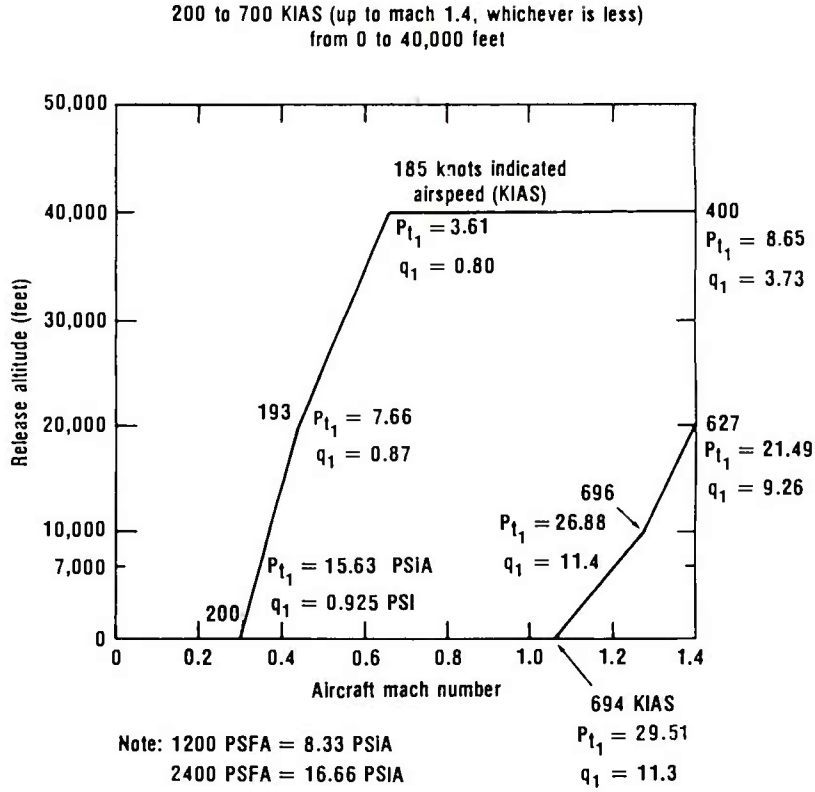

Figure 40. Operational envelope for high drag bomb.

Figure 37 indicates the relation of voltage output versus Mach number for a worst-case condition at an angle of attack of 8 deg. Table 3 and figure 37 show that at the minimum value of q_1 of 0.8, which occurs between Mach 0.25 and 0.3, at a total pressure of 16.66 psia, the turn-on threshold voltage of 15 V is achieved at +8 deg angle of attack. In summary, the wind tunnel data show that the fluidic generator produces voltages above the required threshold voltage for angles of attack up to +8 deg and for the lowest release velocities of the flight envelope.

TABLE 3. WIND TUNNEL CONDITIONS

P_{t_1} (total pressure) (PSIA)	Mach number	Indicated airspeed (international knots)	q_1 Free stream dynamic pressure (PSI)
8.33	0.2	98	0.226
8.33	0.3	144	0.49
8.33	0.4	188	0.83
8.33	0.5	228	1.23
16.66	0.2	138	0.45
16.66	0.3	204	0.986
16.66	0.4	266	1.66
16.66	0.5	323	2.45

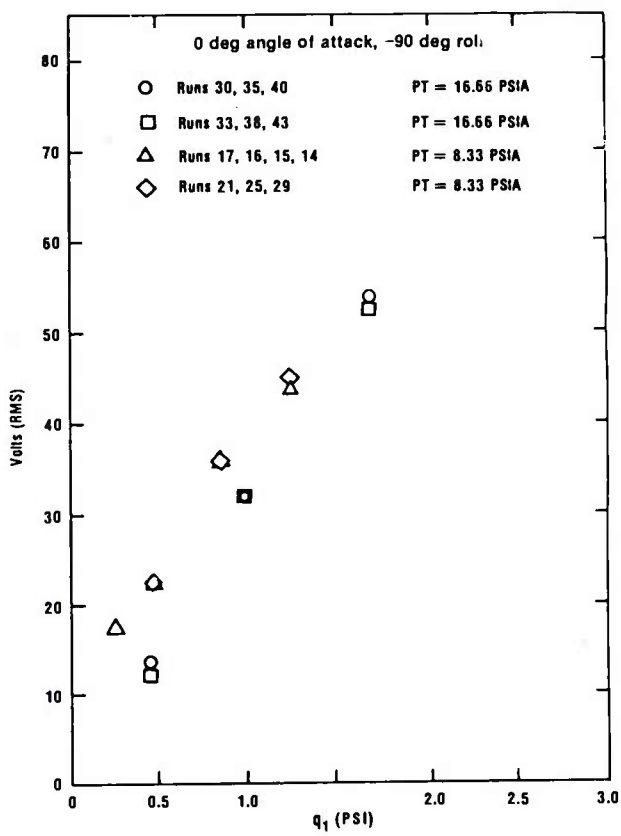

Figure 41. Comparison of voltage values at q for repeated runs.

8. EFFECT OF CONTINUOUS OPERATION IN WIND TUNNEL ON FLUIDIC GENERATOR PERFORMANCE

To verify that the fluidic generator performance had not degraded during continuous operation in the wind tunnel, at the end of the test the Mach number and total pressure conditions were repeated at runs with the bomb at 0 deg angle of attack and the fuze in the -90 deg roll position.

The voltage outputs at the indicated test runs are shown in figure 41 versus free stream dynamic pressure q_1. Each point corresponds to a single run. Voltages measured at the same values of q_1 and total pressure were the same within 1 V. Hence, no degradation was evident in fluidic generator performance during the total duration of the wind tunnel test.

9. SUMMARY AND CONCLUSIONS

The fluidic generator developed for the MLRS rocket fuze power supply was modified to power a modular fuze for Air Force bombs, including high drag bombs. There were efforts to increase the output voltage at low velocity. The generator output then was optimized to compensate for differences in the flow pattern between the Air Force pop-up housing and the MLRS ogive. As a result of this development effort, 28 units were evaluated and delivered to the Air Force for further testing. In the fuze configuration housing these units produced the required 1 W at 1 psig and 2 W at 2 psig.

A wind tunnel test of the generator mounted as intended for use on the MK-84, GBU-10C/B bomb was conducted at Arnold Engineering Center. The purpose was to verify generator performance at the worst-case conditions of the bomb release envelope and to determine the pressure available to the generator at these conditions.

Pressure measurements from a rake installed above a fairing identical to the fuze showed that the pop-up housing was located within the boundary layer. This condition did not lower the generator output below the threshold needed to power the fuze. However, improved performance could be achieved by raising the pop-up inlet by at least 0.50 in. above its present value of 0.90 in. Comparison of pressure measured in the housing with free stream dynamic pressure showed that the pressure recovery (defined as the fraction of the free stream dynamic pressure that appears across the generator) is independent of total pressure, but decreases with angle of attack.

The wind tunnel test covered the low speed portion of the aircraft release envelope for which indicated airspeeds vary from 185 to 200 knots and free stream dynamic pressure changes from 0.8 to 1.0 psi. The voltage measurements for the expected range of flight attitudes showed that the fluidic generator provides voltage above the threshold value for attack angles up to +8 deg and dynamic pressures as low as 0.8 psi (5.5 kPa).

Come-up time measurements show that the fluidic generator provides adequate voltage to arm the fuze well in advance of the required arming time at the minimum airspeed condition.

ACKNOWLEDGEMENTS

The authors wish to acknowledge the contributions of the following individuals: Leroy Hughes of Harry Diamond Laboratories, for testing and evaluating fluidic generator performance during the development effort; R. W. Hobbs (Calspan Field Services), for his assistance in wind tunnel instrumentation and in compiling the wind tunnel data; and Brad Biggs (Motorola), who provided the fuze simulation and circuitry for the wind tunnel test.

LITERATURE CITED

(1) Richard L. Goodyear and Henry Lee, Performance of the Fluidic Power Supply for the XM445 Fuze in Supersonic Wind Tunnels, Harry Diamond Laboratories, HDL-TM-81-4 (February 1981).

(2) Carl J. Campagnuolo and Henry C. Lee, Development of a High-Power Fluidic Generator for Hard-Structure Munitions (HSM) Bomb, Harry Diamond Laboratories, HDL-TR-1988 (May 1982).

(3) Jonathan E. Fine, Performance of Ram Air Driven Power Supply for Proposed High Altitude Rocket in Naval Surface Weapons Center Supersonic Wind Tunnel, Harry Diamond Laboratories, HDL-TM-80-31 (November 1980).

(4) R. W. Hobbs, Wind Tunnel Tests of a Modular Fuze at Mach Numbers from 0.20 to 0.50, Arnold Engineering Development Center, AEDC-TSR-82-P7 (March 1982).

(5) Test Facilities Handbook (Eleventh Edition), Propulsion Wind Tunnel Facility, 4 (April 1981).

(6) R. B. Abernethy and J. W. Thompson, Jr., Handbook--Uncertainty in Gas Turbine Measurements Arnold Engineering Development Center, AEDC-TR-73-5 (February 1973) AD 755 356.

DISTRIBUTION

ADMINISTRATOR
DEFENSE TECHNICAL INFORMATION
CENTER
ATTN DTIC-DDA (12 COPIES)
CAMERON STATION, BUIDING 5
ALEXANDRIA, VA 22314

COMMANDER
US ARMY RSCH & STD GP (EUR)
ATTN CHIEF, PHYSICS & MATH
BRANCH
FPO NEW YORK 09510

COMMANDER
US ARMY ARMAMENT MATERIEL
READINESS COMMAND
ATTN DRSAR-LEP-L, TECHNICAL LIBRARY
ATTN DRSAR-ASF, FUZE & MUNITIONS
SUPPORT DIV
ROCK ISLAND, IL 61299

COMMANDER
US ARMY MISSILE & MUNITIONS
CENTER & SCHOOL
ATTN ATSK-CTD-F
REDSTONE ARSENAL, AL 35809

DIRECTOR
US ARMY MATERIEL SYSTEMS ANALYSIS
ACTIVITY
ATTN DRXSY-MP
ABERDEEN PROVING GROUND, MD 21005

US ARMY ELECTRONICS TECHNOLOGY
& DEVICES LABORATORY
ATTN DELET-DD
FT MONMOUTH, NJ 07703

COMMANDING OFFICER
NAVAL TRAINING EQUIPMENT CENTER
ATTN TECHNICAL LIBRARY
ORLANDO, FL 32813

ENGINEERING SOCIETIES LIBRARY
ATTN ACQUISITIONS DEPARTMENT
345 EAST 47TH STREET
NEW YORK, NY 10017

AMES LABORATORY
DEPT OF ENERGY
IOWA STATE UNIVERSITY
ATTN ENVIRONMENTAL SCIENCES
AMES, IA 50011

BROOKHAVEN
DEPT OF ENERGY
ASSOCIATED UNIVERSITIES, INC
ATTN TECHNICAL INFORMATION DIV
ATTN PHYSICS DEPT, 5103
UPTON, LONG ISLAND, NY 11973

DEPARTMENT OF COMMERCE
NATIONAL BUREAU OF STANDARDS
CENTER FOR RADIATION RESEARCH
WASHINGTON, DC 20230

DEPARTMENT OF ENERGY
ALBUQUERQUE OPERATIONS OFFICE
PO BOX 5400
ALBUQUERQUE, NM 87115

NATIONAL OCEANIC & ATMOSPHERIC ADM
ENVIRONMENTAL RESEARCH LABORATORIES
ATTN LIBRARY, R-51, TECH REPORTS
BOULDER, CO 80302

DIRECTOR
DEFENSE ADVANCED RESEARCH
PROJECTS AGENCY
ARCHITECT BLDG
ATTN MATERIALS SCIENCES
ATTN ADVANCED CONCEPTS DIV
ATTN TARGET ACQUISITION
& ENGAGEMENT DIV
ATTN WEAPONS TECH & CONCEPTS DIV
1400 WILSON BLVD
ARLINGTON, VA 22209

DIRECTOR
DEFENSE COMMUNICATIONS ENGINEERING
CENTER
ATTN TECHNICAL LIBRARY
1860 WIEHLE AVE
RESTON, VA 22090

DIRECTOR
DEFENSE INTELLIGENCE AGENCY
ATTN DT-2, WEAPONS & SYSTEMS DIV
WASHINGTON, DC 20301

DIRECTOR
DEFENSE NUCLEAR AGENCY
ATTN TISI, SCIENTIFIC INFORMATION DIV
WASHINGTON, DC 20305

UNDER SECRETARY OF DEFENSE
FOR RESEARCH & ENGINEERING
ATTN TEST & EVALUATION
ATTN RESEARCH & ADVANCED TECH
WASHINGTON, DC 20301

OUSDR&E
DIRECTOR ENERGY TECHNOLOGY OFFICE
THE PENTAGON
WASHINGTON, DC 20301

OUSDR&E
ASSISTANT FOR RESEARCH
THE PENTAGON
WASHINGTON, DC 20301

DIRECTOR APPLIED TECHNOLOGY LABORATORY
AVRADCOM
ATTN DAVDL-ATL-TSD, TECH LIBRARY
FT EUSTIS, VA 23604

COMMANDER
US ARMY ARMAMENT RESEARCH &
DEVELOPMENT COMMAND
ATTN DRDAR-FU, PROJECT MGT PROJECT OFC
ATTN DRCPM-CAWS, PM, CANNON ARTILLERY
WEAPONS SYSTEMS/SEMI-ACTIVE
LASER GUIDED PROJECTILES
ATTN DRCPM-SA, PM, SELECTED AMMUNITION
ATTN DRDAR-TDS, SYSTEMS DEV &
ENGINEERING
ATTN DRDAR-LC, LARGE CALIBER WEAPON
SYSTEMS LABORATORY
DOVER, NJ 07801

COMMANDER/DIRECTOR
ATMOSPHERIC SCIENCES LABORATORY
US ARMY ERADCOM
ATTN DELAS-AS, ATMOSPHERIC SENSING DIV
ATTN DELAS-BE, BATTLEFIELD ENVIR DIV
ATTN DELAS-BR, ATMOSPHERIC EFFECTS BR
WHITE SANDS MISSILE RANGE, NM 88002

PRESIDENT
US ARMY AVIATION BOARD
ATTN ATZQ-OT-CO, TEST CONCEPT &
OPERATIONS DIV
ATTN ATZQ-OT-CM, CONCEPT &
METHODOLOGY BR
FT RUCKER, AL 36360

DIRECTOR
US ARMY BALLISTIC RESEARCH LABORATORY
ATTN DRDAR-BLT, TERMINAL BALLISTICS DIV
ABERDEEN PROVING GROUND, MD 21005

COMMANDER
USARRADCOM
BENET WEAPONS LAB LCWSL
WATERVLIET, NY 12189

COMMANDER/DIRECTOR
CHEMICAL SYSTEMS LABORATORY
ARRADCOM
ATTN DRDAR-CLJ-L, TECHNICAL LIBRARY BR
ABERDEEN PROVING GROUND, MD 21010

COMMANDER/DIRECTOR
COMBAT SURVEILLANCE
& TARGET ACQUISITION LABORATORY
US ARMY ERADCOM
ATTN DELCS-S, DIR SPECIAL SENSORS DIV
FT MONMOUTH, NJ 07703

COMMANDER
COMBAT DEVELOPMENTS
EXPERIMENTATION COMMAND
FT ORD, CA 93941

COMMANDER
US ARMY COMMUNICATIONS & ELECTRONICS
MATERIEL READINESS COMMAND
FT MONMOUTH, NJ 07703

COMMANDER
US ARMY COMMUNICATIONS RESEARCH &
DEVELOPMENT COMMAND
ATTN DRCPM-MSCS, OFC OF THE PM MULTI-
SERVICE COMMUNICATIONS SYS
FT MONMOUTH, NJ 07703

COMMANDER
ERADCOM TECHNICAL SUPPORT ACTIVITY
ATTN DELSD-L, TECH LIB DIR
FT MONMOUTH, NJ 07703

DIRECTOR
ELECTRONICS TECHNOLOGY &
DEVICES LABORATORY
US ARMY ERADCOM
ATTN DELET-DT, DIR TECHNICAL PLANS &
PROGRAMS OFFICE

COMMANDER
WATERVLIET ARSENAL
WATERVLIET, NY 12189

COMMANDER
US ARMY ABERDEEN PROVING GROUND
ATTN STEAP-TL, TECH LIB
ABERDEEN PROVNG GROUND, MD 21005

COMMANDER
US ARMY ELECTRONICS PROVING GROUND
FT HUACHUCA, AZ 85613

COMMANDER
US ARMY YUMA PROVING GROUND
YUMA, AZ 85364

COMMANDANT
US ARMY FIELD ARTILLERY SCHOOL
ATTN LIBRARY
FT SILL, OK 73503

COMMANDANT
US ARMY ENGINEER SCHOOL
ATTN LIBRARY
FT BELVOIR, VA 22060

COMMANDANT
US ARMY INFANTRY SCHOOL
ATTN LIBRARY
FT BENNING, GA 31905

COMMANDANT
US ARMY WAR COLLEGE
ATTN LIBRARY
CARLISLE BARRACKS, PA 17013

COMMANDER
US ARMY ORDNANCE
CENTER & SCHOOL
ABERDEEN PROVING GROUND, MD 21005

ASSISTANT SECRETARY OF THE NAVY
RESEARCH, ENGINEERING, & SYSTEMS
DEPT OF THE NAVY
WASHINGTON, DC 20350

COMMANDER
NAVAL AIR DEVELOPMENT CENTER
ATTN TECHNICAL LIBRARY
WARMINSTER, PA 18974

COMMANDER
NAVAL AIR SYSTEMS COMMAND HQ
DEPT OF THE NAVY
WASHINGTON, DC 20361

SUPERINTENDENT
NAVAL POSTGRADUATE SCHOOL
ATTN LIBRARY, CODE 2124
MONTEREY, CA 93940

DIRECTOR
NAVAL RESEARCH LABORATORY
ATTN 2600, TECHNICAL INFO DIV
WASHINGTON, DC 20375

CHIEF OF NAVAL RESEARCH
DEPT OF THE NAVY
ATTN ONR-400, ASST CH FOR RES
ARLINGTON, VA 22217

COMMANDER
NAVAL SHIP ENGINEERING CENTER
WASHINGTON, DC 20360

COMMANDER
DAVID W. TAYLOR NAVAL SHIP R&D CENTER
BETHESDA, MD 20084

COMMANDER
NAVAL SURFACE WEAPONS CENTER
ATTN DX-21 LIBRARY DIV
DAHLGREN, VA 22448

COMMANDER
NAVAL SURFACE WEAPONS CENTER
ATTN X-22, TECHNICAL LIB
WHITE OAK, MD 20910

COMMANDER
NAVAL WEAPONS CENTER
ATTN 38, RESEARCH DEPT
ATTN 381, PHYSICS DIV
CHINA LAKE, CA 93555

COMMANDING OFFICER
NAVAL WEAPONS EVALUATION FACILITY
KIRTLAND AIR FORCE BASE
ALBUQUERQUE, NM 87117

ELECTRONICS TECHNOLOGY &
DEVICES LABORATORY (Cont'd)
ATTN DELET-E, DIR ELECTRONIC MATERIALS
RESEARCH DIV
FT MONMOUTH, NJ 07703

DIRECTOR ELECTRONIC WARFARE LABORATORY
ATTN DELEW-V, EM VULN & ECCM DIV
FT MONMOUTH, NJ 07703

PRESIDENT
US ARMY FIELD ARTILLERY BOARD
ATTN ATZR-BDWT, WEAPONS TEST DIV
FT SILL, OK 73503

PRESIDENT
US ARMY INFANTRY BOARD
ATTN ATZB-IB-AT, ANTIARMOR TEST DIV
FT BENNING, GA 31905

COMMANDER
US ARMY MATERIALS & MECHANICS
RESEARCH CENTER
ATTN DRXMR-PL, TECHNICAL LIBRARY
ATTN DRXMR-T, MECHANICS & ENGINEERING
LABORATORY
ATTN DRXMR-E, METALS & CERAMICS
LABORATORY
WATERTOWN, MA 02172

COMMANDER
US ARMY MISSILE COMMAND
ATTN DRCPM-RS, GENERAL SUPPORT
ROCKET SYS (5 COPIES)
ATTM DRSMI-U, WEAPONS SYST MGT DIR
ATTN DRSMI-S, MATERIEL MANAGEMENT
REDSTONE ARSENAL, AL 35809

DIRECTOR
US ARMY MISSILE LABORATORY
USAMICOM
ATTN DRSMI-RPT, TECHNICAL
INFORMATION DIV
ATTN DRSMI-RA, CHIEF, DARPA PROJECTS
OFFICE
ATTN DRSMI-RR, RESEARCH DIR
ATTN DRSMI-RE, ADVANCED SENSORS DIR
REDSTONE ARSENAL, AL 35809

COMMANDER & DIRECTOR OFC OF MISSILE
ELCT WARFARE
ATTN DELEW-M-ST, SURFACE TARGET DIV
WHITE SANDS MISSILE RANGE, NM 88002

DIRECTOR
NIGHT VISION & ELECTRO-OPTICS
LABORATORY
ATTN DELNV-AC, ADVANCED CONCEPTS DIV
ATTN DELNV-SE, MISSILES
ATTN DELNV-VI, BATTLEFIELD ENVIRONMENT
FT BELVOIR, VA 22060

DIRECTOR
PROPULSION LABORATORY
RESEARCH & TECHNOLOGY LABORATORIES
AVRADCOM
LEWIS RESEARCH CENTER, MS. 106-2
21000 BROOKPARK ROAD
CLEVELAND, OH 44135

DIRECTOR
US ARMY RESEARCH & TECHNOLOGY
LABORATORIES
AMES RESEARCH CENTER
MOFFETT FIELD, CA 94035

US CHIEF ARMY RESEARCH OFFICE (DURHAM)
PO BOX 12211
ATTN DRXRO-MS, METALLURGY-MATERIALS
DIV
RESEARCH TRIANGLE PARK, NC 27709

DIRECTOR RESEARCH & TECHNOLOGY
LABORATORIES (AVRADCOM)
AMES RESEARCH CENTER
MOFFETT FIELD, CA 94035

OFFICE OF THE DEPUTY CHIEF OF STAFF
FOR RESEARCH, DEVELOPMENT, & ACQUISITION
ATTN DIR OF ARMY RES, DAMA-ARZ-A
DR. M. E. LASSER
ATTN DAMA-ZE, ADVANCED CONCEPTS TEAM
ATTN DAMA-WSA, AVIATION SYSTEMS DIV
WASHINGTON, DC 20310

COMMANDER
WHITE SANDS MISSILE RANGE
DEPT OF THE ARMY
ATTN STEWS-CE, COMMUNICATIONS/
ELEC OFFICE
WHITE SANDS MISSILE RANGE, NM 88002

COMMANDER
EDGEWOOD ARSENAL
ABERDEEN PROVING GROUND, MD 21005

DEPUTY CHIEF OF STAFF
RESEARCH & DEVELOPMENT
HEADQUARTERS, US AIR FORCE
ATTN AFRDQSM
WASHINGTON, DC 20330

SUPERINTENDENT
HQ US AIR FORCE ACADEMY
ATTN TECH LIB
USAF ACADEMY, CO 80840

AF AERO-PROPULSION LABORATORY
WRIGHT-PATTERSON AFB, OH 45433

COMMANDER
ARNOLD ENGINEERING DEVELOPMENT CENTER
ATTN DY, DIR TECHNOLOGY
ARNOLD AIR FORCE STATION, TN 37389

ARMAMENT DEVELOPMENT & TEST CENTER
EGLIN, AFB
ATTN AD/DLJF, RICHARD MABRY
ATTN AD/DLJ-I, SHARON LEE (5 COPIES)
ATTN AD/DLJ-I, CPT. P. ELLIS (10 COPIES)
ATTN AD/YXM, C. TEW
EGLIN, FL 32542

MOTOROLA G.E.G.
8201 EAST MCDOWELL RD
ATTN BILL MAULE (5 COPIES)
SCOTTSDALE, AZ 85252

CHIEF
FIELD COMMAND
DEFENSE NUCLEAR AGENCY
LIVERMORE DIVISION
PO BOX 808
ATTN FCPRL
ATTN NON NUCLEAR WARHEAD PROJECTS OFFICE
LIVERMORE, CA 94550

COMMANDER
HQ AIR FORCE SYSTEMS COMMAND
ANDREWS AFB
ATTN TECHNICAL LIBRARY
WASHINGTON, DC 20334

AMES RESEARCH CENTER
NASA
ATTN TECHNICAL INFO DIV
MOFFETT FIELD, CA 94035

DIRECTOR
NASA
GODDARD SPACE FLIGHT CENTER
ATTN 250, TECH INFO DIV
GREENBELT, MD 20771

DIRECTOR
NASA
ATTN TECHNICAL LIBRARY
JOHN F. KENNEDY SPACE
CENTER, FL 32899

DIRECTOR
NASA
LANGLEY RESEARCH CENTER
ATTN TECHNICAL LIBRARY
HAMPTON, VA 23665

DIRECTOR
NASA
LEWIS RESEARCH CENTER
ATTN TECHNICAL LIBRARY
CLEVELAND, OH 44135

LAWRENCE LIVERMORE NATIONAL LABORATORY
PO BOX 808
LIVERMORE, CA 94550

SANDIA LABORATORIES
LIVERMORE LABORATORY
PO BOX 969
LIVERMORE, CA 94550

SANDIA NATIONAL LABORATORIES
PO BOX 5800
ALBUQUERQUE, NM 87185

US ARMY ELECTRONICS RESEARCH
& DEVELOPMENT COMMAND
ATTN COMMANDER, DRDEL-CG
ATTN TECHNICAL DIRECTOR, DRDEL-CT
ATTN PUBLIC AFFAIRS OFFICE, DRDEL-IN

HARRY DIAMOND LABORATORIES
ATTN CO/TD/TSO/DIVISION DIRECTORS
ATTN RECORD COPY, 81200
ATTN HDL LIBRARY, 81100 (3 COPIES)
ATTN HDL LIBRARY, 81100 (WOODBRIDGE)
ATTN TECHNICAL REPORTS BRANCH, 81300
ATTN LEGAL OFFICE, 97000
ATTN CHAIRMAN, EDITORIAL COMMITTEE
ATTN MORRISON, R. E., 13500 (GIDEP)
ATTN CHIEF, 21000
ATTN CHIEF, 21100
ATTN CHIEF, 21200
ATTN CHIEF, 21300
ATTN CHIEF, 21400
ATTN CHIEF, 21500
ATTN CHIEF, 22000
ATTN CHIEF, 22100
ATTN CHIEF, 22300
ATTN CHIEF, 22800
ATTN CHIEF, 22900
ATTN CHIEF, 20240
ATTN L. COX, 00211
ATTN G. POPE, 00211
ATTN S. ELBAUM, 97100
ATTN P. KOPETKA, 34600
ATTN N. DOCTOR, 34600
ATTN F. BLODGETT, 34600
ATTN P. INGERSOLL, 34300
ATTN G. NORTH, 47500
ATTN B. WILLIS, 47400
ATTN R. PROESTEL, 34600
ATTN H. DAVIS, 34600
ATTN L. HUGHES, 34600
ATTN M. MCCALL, 34600
ATTN S. ALLEN, 34600
ATTN J. W. MILLER, 34300
ATTN B. GOODMAN, 42440
ATTN M. FLOYD, 47400
ATTN C. SPYROPOULOS, 22100
ATTN C. CAMPAGNUOLO, 34600 (20 COPIES)
ATTN J. FINE, 34600 (10 COPIES)